Virginia Commonwealth University
VCU Scholars Compass

Theses and Dissertations | Graduate School

2019

Modeling the peak absorption of MEH-PPV in various solvents using Density Functional Theory

Corell H. Moore
Virginia Commonwealth University

Follow this and additional works at: https://scholarscompass.vcu.edu/etd

 Part of the Polymer and Organic Materials Commons

© The Author

Downloaded from
https://scholarscompass.vcu.edu/etd/6041

This Thesis is brought to you for free and open access by the Graduate School at VCU Scholars Compass. It has been accepted for inclusion in Theses and Dissertations by an authorized administrator of VCU Scholars Compass. For more information, please contact libcompass@vcu.edu.

Theses and Dissertations Graduate School

2019

Modeling the peak absorption of MEH-PPV in various solvents using Density Functional Theory

Corell Halsey Moore

Virginia Commonwealth University

Modeling the peak absorption of MEH-PPV in various solvents using Density Functional Theory

A dissertation submitted in partial fulfillment of the requirements for the degree of Doctor of Philosophy at Virginia Commonwealth University

by Corell Halsey Moore B.S. Mechanical Engineering, Duke University, 1984

M.S. Mathematics, Virginia Commonwealth University, 2004

Director: Dr. Gary Tepper, Professor and Chair, Mechanical and Nuclear Engineering

Contents

List of Figures:

List of Tables:

Abstract

Modeling the peak absorption of MEH-PPV in various solvents using Density Function Theory

By Corell Halsey Moore

A dissertation submitted in partial fulfillment of the requirements for the degree of Doctor of Philosophy at Virginia Commonwealth University.

Virginia Commonwealth University, 2019

Major Director: Dr. Gary Tepper, Mechanical and Nuclear Engineering

Density Functional Theory (DFT) and time-dependent Density Functional Theory (TD-DFT) are powerful tools for modeling orbital energy in conjugated molecules and have been useful tools for research in organic photovoltaics. In this work, DFT is first used to explain the red shift in the absorption spectrum and increased absorption observed in MEH-PPV. Initially, the modeling of the red-shift in the absorption peak of MEH-PPV is studied using Gaussian 03 software with the global hybrid functional B3LYP for exchange-correlation and the 6-31G basis set. DFT and TD-DFT are used to separately study the effects of polymer chain length, carbon-carbon double-bond stretching, and the polymer in solution vs. in gas space on red shift in absorption spectrum.

Next, Gaussian 09 software and the same B3LYP functional and 6-31G basis set are used to study interchain and intrachain interactions of MEH-PPV in solution. The red shift

in the absorption peaks for three MEH-PPV configurations (single-chain pentamer, two stacked pentamers, and decamer) are compared with experimental results for five different solvents (chloroform, toluene, xylene, dichloromethane, and chlorobenzene). This investigation indicates that inter-chain interactions dominate in "good" aromatic solvents as compared to "poor" non-aromatic solvents. The results suggest that inter-chain charge transfer interactions play a critical role in real solutions and inter-chain aggregation takes precedence over intra-chain aggregation in aromatic solvents.

In the final section of the study, accurate values for the range-separation parameter (ω) for three lengths of MEH-PPV polymer (trimer, tetramer, and pentamer) in five different solvents (chloroform, chlorobenzene, xylene, Tetrahydrofuran, and dichloromethane) are reported using the range-separated functionals wB97XD and CAM-B3LYP. Using these data, range separation parameters are predicted and used for longer polymer chains in chloroform solution. The differences in the range separation parameters for the different solvents is statistically significant and gives further insight into the polymer/solvent interaction.

Chapter 1

Introduction

More than 80% of the world's current energy needs are met by fossil fuels. With a growing world population and rising standard of living in the developing world, there is an increasing demand for energy. Due to the limited sources of fossil fuels and their adverse effect on the environment due to CO_2 emissions, it is only matter of time before the world faces an energy crisis. According to the U.S. Energy Information Administration, world energy consumption will increase from 524 quadrillion Btu in 2010 to 630 quadrillion Btu in 2020 and 820 Btu in 2040. More than 85 percent of the increase in global energy demand from 2010 to 2040 will occur in developing nations [International Energy Outlook 2013]. While energy conservation and efficiency can address some of the issues, to maintain the current economic growth and standard of living without affecting the climate, it is imperative to develop alternative energy sources that are clean, abundant, cost-effective, and safe.

Meeting this demand will require a variety of energy sources such as solar, wind, hydro, biomass, and hydrogen. However, the most viable solution can come from harnessing solar energy which offers an inexhaustible energy source. It is clean and climate friendly. Equally important, its availability is greater in warm and sunny countries where most of the world's population and economic growth over the next decades will occur [Solar Energy perspectives 2011].

Due to the relatively low efficiency and high cost of photovoltaic cells, just 1.6% of U.S. energy is generated from solar [US Energy Information Administration, 2019]. Current research is looking for ways to make solar power more affordable and efficient. Crystalline silicon solar cells currently dominate the solar energy market and although costs for photovoltaic power from silicon solar cells have come down drastically, solar power still has trouble competing with conventional power sources. Polymer solar cells have long been proposed as a lower cost alternative to silicon [Gong, 2012; Saricfici, 1992; Blom, 2007; Huo, 2011; Small, 2013; Po, 2010; Zang, 2003]. However, the efficiencies found with polymer solar cells are severely limited [Small, 2013; Po, 2010; Zang, 2003]. One of the challenges of polymer solar cells is the limited absorption range. Capturing more of the absorption spectrum would enable polymer solar cells to be more efficient and cost effective.

In order to produce electricity, solar cells must absorb light from the solar spectrum. If solar cells absorb more of the solar spectrum, they can produce more electricity. Ultraviolet visible spectroscopy, otherwise known as UV-Vis, refers to absorption spectroscopy or reflectance spectroscopy in the solar spectrum region of visible light as well as part of the ultraviolet region. A UV-Vis spectrophotometer was used to capture absorption data. More detail can be found in Chapter 3.

The motivation for this work began with previous work electrospinning the polymer MEH-PPV. Previous work had observed that when the polymer was electrospun, a red shift in peak absorption occurred. This resulted in an interest in better understanding the sources of the red-shift in peak absorption in MEH-PPV. Capturing more of the light spectrum would benefit the efficiency of polymer solar cells. More detail can be found in Chapter 2.

MEH-PPV is a much-studied polymer used in photovoltaic applications. In an effort to understand shifts in the absorption spectrum of MEH-PPV, the computational chemistry software, Gaussian 09, was used to model the MEH-PPV polymer [Giri, 2014]. The objective of this work was to use both experimental results and computational/theoretical tools to observe what is happening with the polymer. Figure 2.2 shows a monomer unit of MEH-PPV. Experimental data is presented in Chapter 3.

Gaussian 09 computational chemistry software provides state-of-the-art capabilities for electronic structure modeling and uses various methods to solve the Schrodinger equation and predict many properties of atoms, molecules, and reactive systems. Density Functional Theory (DFT) is a powerful method used by Gaussian 09 to solve the Schrodinger equation. The DFT approach uses functionals (functions of another function) to determine the properties of a many-body system. DFT is based on modeling electron correlation via general functionals of the electron density. The details of Gaussian 09 are described in Chapter 4.

One challenge of modelling a polymer is that the length of the polymer can vary by adding more molecules to the polymer chain. Longer conjugation lengths cause the absorption spectrum to red shift [Nguyen,1999; Traiphol, 2010; Collison, 2001; Zhu, 2009]. In addition, when a polymer is used in a solar cell it is placed in a solvent. The solvent is another variable that can affect absorption. More details can be found in Chapter 5.

The absorption performance of conjugated polymer solar cells depends on polymer morphology. Morphology consists of chain conformation and aggregation [Chiu,2012]. Both intra-chain and inter-chain couplings depend on the amount of aggregation [Yamagata

2012]. Intra-chain (through-bond) interactions occur within a given chain and inter-chain (Coulombic) interactions occur between chains. The morphology of polymer chains in solution determines how the chain packing of inter-chain aggregation can be performed. Aggregation causes a red shift in the absorption spectrum. More details can be found in chapter 6.

A model chemistry generally consists of the combination of a theoretical method with a basis set. Each unique pairing of method and basis set represents a different approximation to the Schrodinger equation. To model a complex polymer many factors must be considered in selecting the theoretical method, such as DFT, and the basis set. Functionals used in DFT that are not long range corrected are unable to correctly predict electronic transitions of conjugated systems involving the charge transfer process [Bhatta, 2015] [Korzdorfer, 2011; Avhad, 2017; Borpuzari, 2017; Yanai, 2004; Refaely-Abramson, 2011; Chai, 2008; Sekar, 2018; Pandey, 2012]. Range-separated (RS) functionals have been created to overcome this problem. In RS-functionals, the range separation parameter ω is employed in order to switch between the Density Functional Theory and Hartree-Fock methods for modeling the system. It is important, however, to use an appropriate ω for the molecule being modelled and the RS functional being used. Currently, the appropriate ω is not known for many molecules. Values of ω for polymers are particularly difficult to determine. Optimized values for the range separation parameter when modelling MEH-PPV were determined. More detail can be found in chapter 7. Conclusions can be found in chapter 8.

Chapter 2

Absorption in Solar Cells

2.1 The Solar Spectrum

The direct conversion of light into electricity is known as the photovoltaic effect. Photovoltaic materials absorb photons of light and release electrons. An electric current results when these free electrons are captured. The intensity of sunlight hitting a surface is called irradiance. Irradiance is the sum of the contributions of all wavelengths within the spectrum, expressed in units of Watts per m^2 of a surface. The energy in solar irradiation comes in the form of electromagnetic waves of a wide spectrum. Longer wavelengths have less energy (red-shifted) than shorter ones (blue-shifted). The solar spectrum changes throughout the day and with location. Standard reference spectra are defined to allow the performance comparison of photovoltaic devices from different manufacturers and research laboratories. The standard spectrum for space applications is referred to as AM0. It has an integrated power of 1366.1 $W/m^{2.}$ Two standards are defined for terrestrial use: the AM1.5 Global spectrum (1000 W/m^2) and the AM1.5 Direct spectrum (900 W/m^2). [PVEducation.org, 2019] Figure 2.1 is a graph illustrating the standard solar spectra.

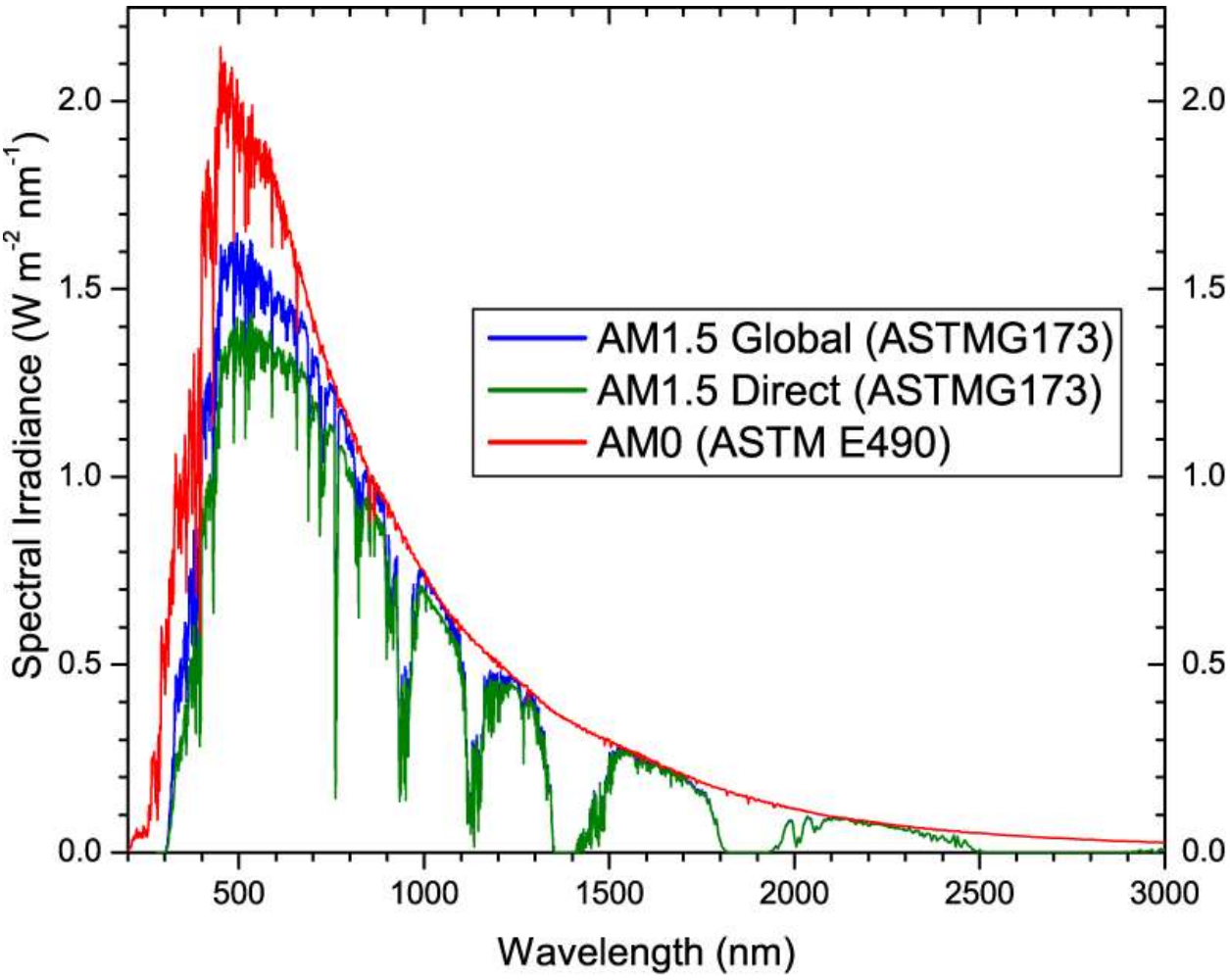

Figure 2.1: Standard Solar Spectra for space and terrestrial use [PV Education.org, 2019]

2.2 Polymer Solar Cells

In order to produce electricity, solar cells must absorb light from the solar spectrum. The most popular material used for solar cells is silicon. 95% of the solar cells on the market today are made of some type of silicon [Fraunhofer Institute, 2019]. Crystalline silicon solar cells currently dominate the solar energy market and although the costs for photovoltaic power from silicon solar cells have come down drastically, solar power still has trouble competing with conventional power sources. Some conjugated polymers also have photovoltaic properties. Conjugated polymers retain the attractive mechanical properties and

processing advantages of polymers and at the same time exhibit the electrical and optical properties of metals or semiconductors [Zhong, 2012; Heeger, 2001]. Polymer solar cells are an alternative to silicon that could make solar cells more affordable. On the positive side, polymer solar cells are lightweight and can be made flexible. These qualities could make new applications possible. On the negative side, polymer solar cells currently have limited efficiency and stability.

2.3 MEH-PPV

The luminescent and semiconducting properties of conjugated polymers based on poly(phenylenevinylene) or PPV have been of much interest for increasing the absorption of polymer solar cells. Of the PPV derivatives, MEH-PPV is of particular interest due to its solubility and ease of fabrication [Tilley,2011]. MEH-PPV consists of a benzene ring with asymmetric alkoxy side chains. The side chains give MEH-PPV its solubility in common organic solvents. This solubility enables the use of techniques such as spin and drop casting [Nguyen, 1999]. MEH-PPV has been extensively studied due to its importance for possible applications in organic light emitting diodes and photovoltaic devices. Figure 2.2 is an optimized MEH-PPV monomer created in the Gaussview software.

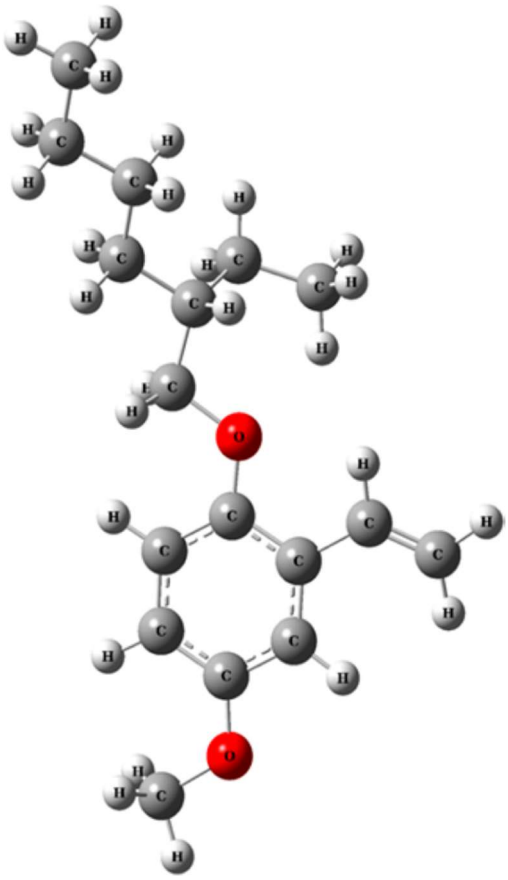

Figure 2.2: Optimized Geometry of MEH-PPV monomer unit

2.4 UV-Vis

Ultraviolet visible spectroscopy, otherwise known as UV-Vis, refers to absorption spectroscopy or reflectance spectroscopy in the solar spectrum region of visible light as well as part of the ultraviolet region. This technique is used to measure the absorption spectrum of various materials. A typical UV-Vis spectrum for MEH-PPV is shown below

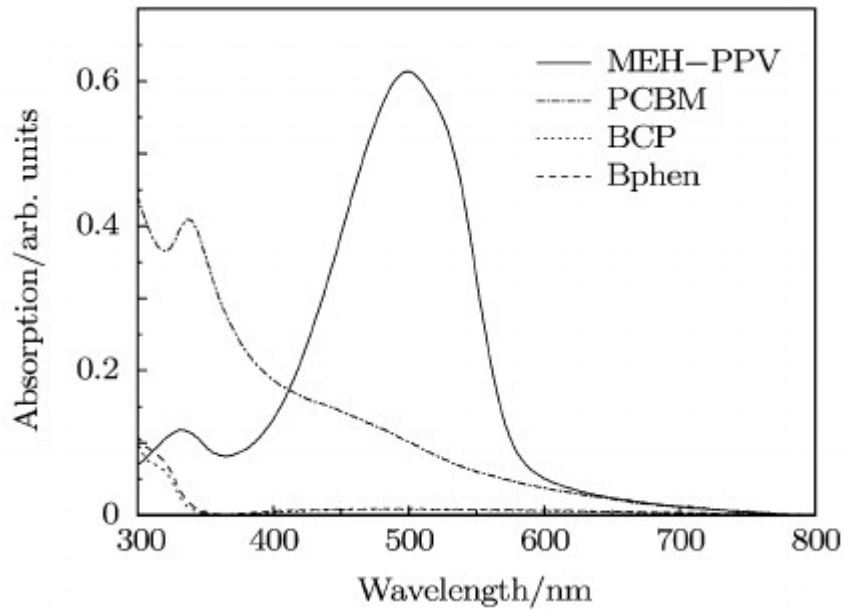

Figure 2.3: Absorption Spectrum of MEH-PPV (solid) [Liu, 2011]

As can been seen in Figure 2.3, MEH-PPV has an absorption peak at around 514 nm. In order to produce more electricity, a solar cell must absorb more of the solar spectrum. This can be achieved by either broadening the absorption spectrum of the solar cell material or by using two materials with different absorption peaks in tandem.

2.5 Electrospinning Study

Previous experiments have found that the peak absorption of MEH-PPV can be red-shifted under certain conditions. For instance, electrospinning uses an electrical charge to extract a very fine fiber from a liquid and can be used to prepare micro and nanofibers from metals, inorganic compounds, and polymers. Studies on electrospun MEH-PPV fibers show a red shift in the absorption peak when compared to spin-cast thin films. In a study by Babel et al (14), the absorption peak of electrospun nanofibers was red-shifted by 30 nm from that of spin-cast thin films. In previous work, various concentrations of MEH-PPV in

chloroform were coaxially electrospun with PVP in our laboratory [Nagata,2013]. After PVP extraction with ethanol, the electrospun MEH-PPV nanofibers were tested by a series of optical characterization methods. A Perkin Elmer model Lamda 40 UV-VIS spectrophotometer was used to study absorption. The absorption peak of the MEH-PPV thin film was measured at 514 nm. A significant red shift to nearly 600 nm was seen in the highest concentration of MEH-PPV electrospun nanofibers. The absorption bands also exhibited broadening with increased concentration [Nagata,2013].

The experimental results illustrating the red-shift in electrospun MEH-PPV polymer are shown in Fig. 3. Solutions of MEH-PPV with 0.24, 0.35, 0.47, and 0.7 weight % concentration in chloroform were coaxially electrospun with PVP as the outer layer. Absorption was measured after PVP extraction with ethanol. It is evident that the peak in the absorption graph shifts to a higher wavelength with increase in MEH-PPV concentration reaching a value of 590 nm as the concentration reaches 0.7 %. The absorption peak of the MEH-PPV thin film obtained from spin casting was found to be 514 nm. This represents a red shift of 76 nm that results from the electrospinning [Nagata,2013].

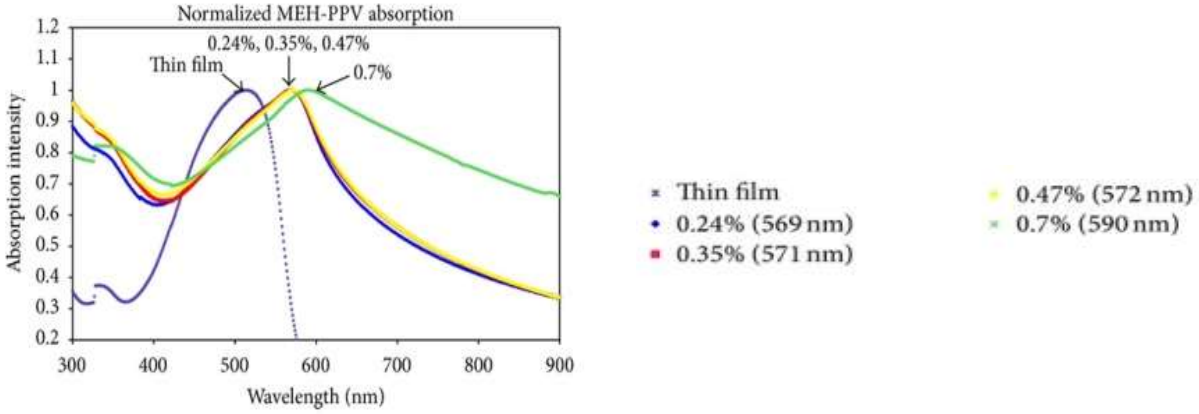

Figure 2.4: MEH-PPV absorption at different concentrations in chloroform solution. [Nagata, 2013]

The initial motivation for the work in this thesis was to understand the origin of the observed red-shift of the absorption peak of electrospun MEH-PPV with the goal of using this increased absorption range to develop more efficient solar cells. Additional research showed that the red-shift could result from any number of factors including conjugation length and solvent used. The next chapter, Chapter 3, shows experimental results demonstrating the effect of conjugation length and solvent on the absorption spectrum peak of MEH-PPV. Then, in an effort to better understand these shifts, the computational chemistry software, Gaussian 09, was used to model the MEH-PPV polymer. The details of Gaussian 09 are described Chapter 4.

Chapter 3

Experimental results

3.1 Previous Studies

Previous work has shown that numerous factors can lead to a shift in the absorption peak of the MEH-PPV polymer. Increased conjugation length has been shown to result in a red-shift [Nguyen, 1999; Traiphol, 2010; Collison, 2001; Zhu, 2009]. Previous studies have also shown that the solvent can affect polymer morphology and conjugation length. "Poor" solvents like terahydrofuran (THF) have been shown to cause collapsing and kinking of the polymer chain which can break the conjugation length. A study by Potai et al found the absorption peak for MEH-PPV in solution with THF to be 503 nm and in Dichloromethane (DCM) to 507 nm. This red shift was attributed to DCM forming extended chains in the DCM solution and forming collapsed chains in the THF solution [Potai, 2013]. A study by Quan et al also saw greater conformational disorder in THF than in toluene [Quan, 2005]. A study by Zheng et al found a trend that there is a slight red shift of the absorption spectra in aromatic solvents compared with that in aliphatic solvents which have the same polarity [Zheng, 1998]. THF is an aliphatic solvent. The interactions of MEH-PPV and solvents are mainly caused by the dipole-dipole interaction. THF is a fairly polar solvent, so it is likely that the weak-polar polymer is more kinked in these polar solvents.

Aggregation, in which chromophores interact electronically, has also been shown to cause a red shift in the absorption spectra, but there is disagreement as to how much this effects optical property. A study by So et al indicates that aggregates in polymer films

enhance charge transport [So, 2012]. A study by Zayana et al used non-aromatic solvents (chloroform and THF) as well as aromatic solvents (toluene and xylene) to find UV-Vis spectra for MEH-PPV thin films. Thin films prepared from toluene and xylene slightly red-shifted compared to the films using chloroform and THF. The shifting was explained by aggregation formed in thin films [Zayana, 2013]. A study by Fazlinashatul claimed the conformation of polymer chains in thin films can be controlled by the selection of organic solvents. The aromatic solvents (xylene and toluene) were shown to give optimum performance for both electrical and optical properties compared to poor performance of non-aromatic solvents (THF and chloroform) [Fazlinashatul, 2011]. Additional studies have shown that the effect of the solvent continues from solution to thin films. A study by Chiu et al discussed the fact that optical electronic properties of conjugated polymers are sensitive to the polymer morphology in solution-cast thin films. The morphology depends on the polymer conformations in the solution phase [Chiu, 2012]. On the other hand, a study by Lampert et al compared MEH-PPV spin cast films in both chlorobenzene (CB) and tetrahydrofuran (THF). CB was chosen because of its known ability to promote aggregate formation, while THF is known to effectively limit aggregate formation. Their results claimed that the degree of aggregation in the films as controlled by the solvent has minimal impact on the net optical gain properties of spin cast MEH-PPV films [Lampert, 2012].

3.2 UV-Vis spectrophotometer and the Beer Lambert Law

In order to better understand the reasons for the red-shift, more accurate experimental results were needed specifically showing the effects of solvent and chain length on absorption. Initially, in order to study solvent effects on the absorption spectrum, solutions of MEH-PPV in five different solvents were studied experimentally using the Cary Model 6000i UV-Vis spectrophotometer. Commercially available MEH-PPV was obtained from Sigma-Aldrich with a molecular weight of 70,000-100,000 g/mol [Product Number: 541435, CAS Number 138184-36-8]. The solvents used were Chloroform, Chlorobenzene, Dichloromethane, Toluene, and Xylene. Each of these is known to be a solvent for MEH-PPV. A 0.002 weight percent solution was made of MEH-PPV in each solvent. Molar absorptivity and the concentration are determined by the Beer-Lambert Law. The Beer-Lambert law states:

$$A = log_{10} \frac{I_0}{I} = \varepsilon lc \qquad 3.1$$

where:

A=Absorbance

I_0=Intensity of Light passing through the reference cell (for each wavelength)

I=Intensity of Light passing through the sample cell (for each wavelength)

ε=molar absorptivity (molar absorption coefficient)

l=length of solution the light passes through (cm)

c=concentration of solution [Clark, 2007]

Molar Absorptivity is dependent on the solvent and the polymer. Therefore, it can be expected that the absorption depends on both the solvent and the polymer concentration. In order to have reliable UV-Vis graphs, the peak Absorbance (A) must equal or be close to one. Therefore, the solutions tested needed to be dilute solutions where concentration was low. The UV-Vis graphs for the experimental data using commercial MEH-PPV are shown in Figure 2. The peak absorption wavelengths are also given in Table 1

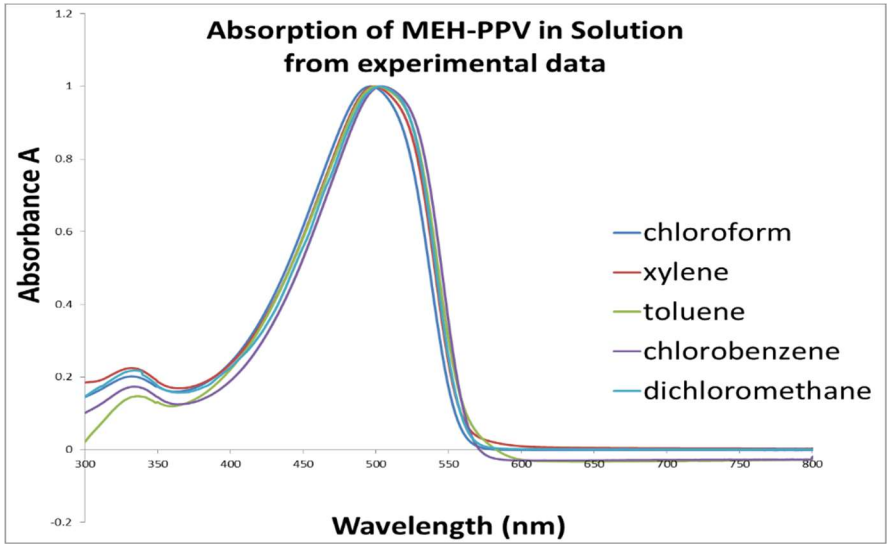

Figure 3.1 Experimental UV-Vis graphs of MEH-PPV in five solvents

It can be seen from Figure 3.1 and from the last line of Table 3.1 that changing the solvent results in a small change in the peak absorption wavelength. However, the results also highlight two potential issues. First, for commercially available MEH-PPV, the conjugation length of the polymer chains in solution is unknown. It is well known that the polymer conjugation length affects the absorption and that the absorption peak red shifts as the conjugation length becomes longer [Nguyen, 1999; Traiphol, 2010; Collison, 2001, Zhu,

2009]. In order to improve the accuracy of the computational model, new UV-VIS experimental data for MEH-PPV chain lengths of exactly 3, 4, and 5 monomers, (trimer, tetramer, and pentamer) in five solvents was provided by researchers at the University of Melbourne. (Table 3.1) The trimer, tetramer, and pentamer chains were prepared by sequential Horner-Wadsworh-Emmons reactions [Tilley,2011]. Peak absorption data was found using a Varian Cary 50 Bio UV-Vis Spectrophotometer and plotted in Fig. 3.1.

Table 3.1: Experimental UV-Vis Data for MEH-PPV trimer, tetramer, and pentamer and in solution

Solvent	**Chlorobenzene**	**DCM**	**Chloroform**	**THF**	**Xylene**
Trimer	400.035 nm	396.94 nm	396.94 nm	396.94 nm	396.94 nm
Tetramer	435.036 nm	433.037 nm	431.96 nm	429.96 nm	433.037 nm
Pentamer	458.057 nm	454.075 nm	454.057 nm	451.93 nm	454.995 nm
Commercial	504 nm	503 nm	496 nm	497 nm	500 nm

The second issue highlighted by the data is Figure 3.1 is whether the differences in the peaks due to the different solvents were statistically significant and if so, what is the source of these differences. The data in Table 3.1 for different chain lengths continues to show a difference in absorption peak for different solvents. The wavelength accuracy for the Varian Cary 50 Spectrophotometer is +/-0.07 at 541.94 nm with a reproducibility of +/-0.01nm [Varian Cary 50 specification sheet]. Figure 3.2 illustrates the accuracy of the experiments using error bars.

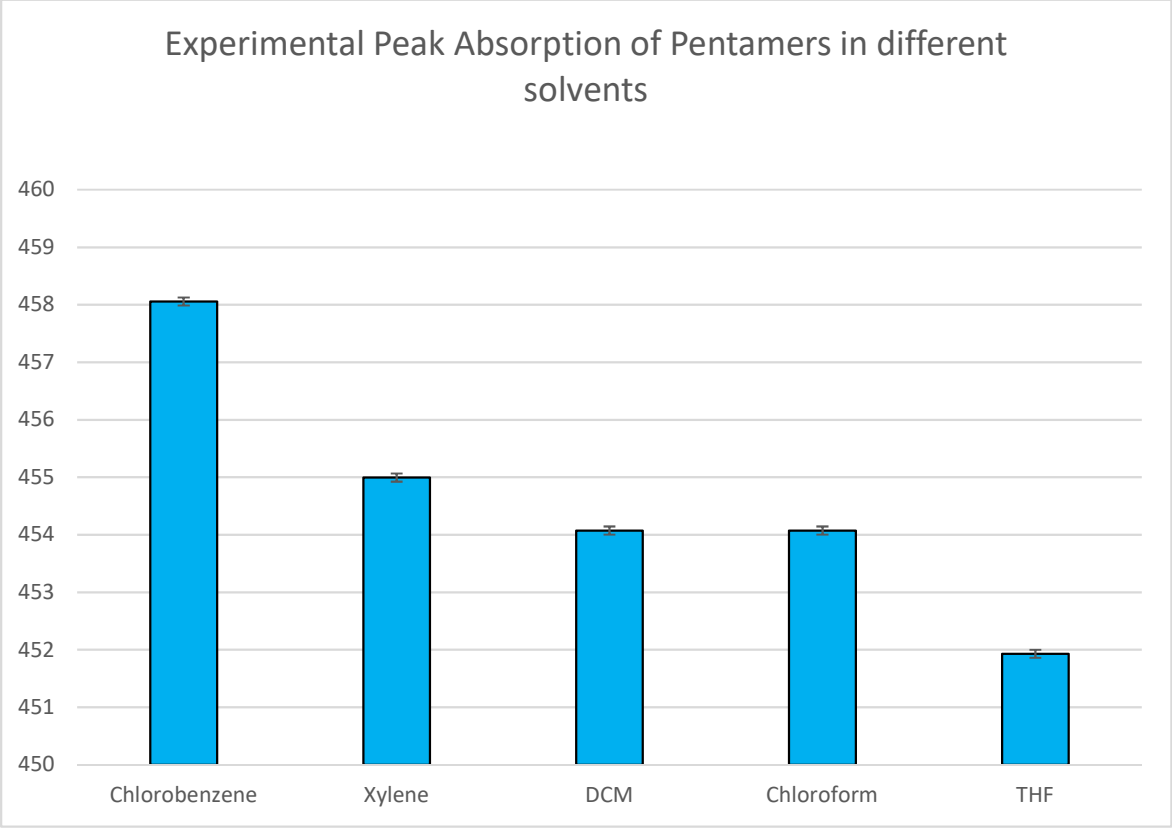

Figure 3.2: Experimental peak absorption of MEH-PPV pentamer in five solvents with error bars

In summary, several things can be seen from the data listed in Table 3.1. First, as expected [Nguyen, 1999; Traiphol, 2010; Collison, 2001; Zhu, 2009], the absorption peak red-shifts as the length of the polymer chain increases. Second, the absorption peak of the Commercial MEH-PPV is far greater than that of the pure pentamer. Finally, the absorption peak varies slightly with the solvent. Although the differences are very small relative to the changes that occur with chain length, the differences in peak absorption with varying solvent are significant, based on the accuracy of the instrument.

With this precise experimental data in hand, the next step was to develop a simulation to accurately model the data. The simulation was built using the Gaussian 09 software which is described in the next chapter.

Chapter 4

Computational Modeling

4.1 Gaussian/DFT

Quantum mechanics explains how entities like electrons have both particle-like and wave-like characteristics. Quantum mechanics specifies that an electron's location is not deterministic but instead consists of a probability density. The Schrodinger Equation describes the wavefunction of a particle (or collection of particles like in a molecule). The energy and many other properties of the particle or collection of particles can be obtained by solving the Schrodinger equation for the wavefunction, subject to the appropriate boundary conditions. Many different wavefunctions are solutions, each corresponding to different states of the system. The solution with the lowest energy is called the ground state. An exact solution to the Schrodinger equation is not possible except for the most trivial molecular systems. However, a number of simplifying assumptions and procedures make an approximate solution possible for a large range of molecules [Foresman, 1993].

Ab initio molecular orbital theory is concerned with predicting the properties of atomic and molecular systems using approximation techniques to solve the Schrodinger equation. The standard and least expensive ab initio approach is called Hartree Fock (HF). HF uses an approximation to create the wavefunction using a determinant that mixes all the orbitals of all the electrons in the molecular system. Hartree-Fock theory provides an inadequate treatment of the correlation between motions of the electrons within a molecular

system, especially those arising between electrons of opposite spin. DFT calculations require approximately the same amount of computational resources as Hartree-Fock. DFT methods are attractive because they include the effects of electron correlation. Electron correlation can be thought of as the fact that electrons in a molecular system react to each other's motion and attempt to stay out of the way of each other. HF calculations incorporate this effect only in an average sense where each electron sees and reacts to an averaged electron density. Since DFT methods include electron correlation they account for instantaneous interactions of pairs of electrons with opposite spin. [Foresman, 1993]

A model chemistry can be described as "an unbiased, uniquely defined, and uniformly applicable model for predicting the properties of a chemical system" [Foresman, 1993]. A model chemistry generally consists of the combination of a theoretical method with a basis set. Each unique pairing of method and basis set represents a different approximation to the Schrodinger equation. The theoretical calculations in this work were performed using Gaussian 03 and Gaussian 09 computational chemistry software. In Gaussian, the user must specify both a theoretical method and a basis set used to perform the theoretical calculations [Foresman, 1993]. The Hartree-Fock method and Density Functional Theory (DFT) are examples of the theoretical methods used to model molecular systems. B3LYP, CAM-b3LYP and wB97XD are examples of functionals which specify how each theoretical method is incorporated [Foresman, 1993]. A basis set is a mathematical representation of the molecular orbitals within a molecule. The basis set can be interpreted as restricting each electron to a specific region of space. Larger basis sets impose fewer constraints on electrons and more accurately approximate exact molecular orbitals. Larger basis sets require more computational resources [Foresman,1993].

Both Hartree-Fock and DFT use the Born-Oppenheimer Approximation to simplify the general molecular problem by separating nuclear and electronic motions. All methods attempt to approximately solve the Schrodinger equation. Hartree-Fock assumes that the wavefunction can be approximated by a single Slater determinant made up of one spin orbital per electron. The Hartree-Fock method does a poor job of handling the correlation between the motion of electrons in a molecular system. Electrons spinning in opposite directions are particularly problematic for Hartree-Fock [Foresman, 1993]. Because of this, resulting energies tend to be too high.

Unlike in Hartree-Fock, in DFT, the many-electron wavefunction is completely bypassed in favor of the electron density. The best DFT methods achieve significantly greater accuracy than Hartree-Fock theory at only a modest increase in cost. DFT uses functionals (functions of another function) to determine the properties of many-body systems. Functions of the spatially dependent electron density function are used for DFT functionals. DFT was thought to be too inaccurate for quantum chemistry calculations until the 1990s. At this time approximations used in the theory were greatly refined to better model the exchange and correlation interactions.

Current DFT methods partition electronic energy into several terms:

$$E=E^{T}+E^{V}+E^{J}+E^{XC} \qquad 4.1$$

Where E^{T} is the kinetic energy term from the motion of electrons, E^{V} is the potential energy from the nuclear-electron attraction and the repulsion between pairs of nuclei, E^{J} is the electron-electron repulsion term (Coulomb self-interaction of the electron density), and E^{XC} is the exchange-correlation term which includes the remaining part of the electron-

electron interactions. All the terms except the nuclear-nuclear repulsion are functions of the electron density [Foresman, 1993].

Hartree-Fock methods exactly treat exchange correlation but have difficulties recovering dynamic electron correlation. DFT has an exact form for dynamic electron correlation but must approximate exchange correlation.

4.2 DFT Functionals

Functionals used in DFT have been defined by the way they treat the exchange and correlation components. A functional is defined in mathematics as a function of a function. In DFT, functionals are functions of the electron density. Electron Density is a function of coordinates in real space [Foresman 1993].

Hybrid functionals are a combination of Hartree-Fock and DFT. Hybrid functionals incorporate a portion of exact exchange from Hartree-Fock theory into the exchange-correlation energy. Hybrid functionals define the exchange functional as a linear combination of Hartree-Fock, local, and gradient-corrected exchange terms. The correlation functional has no Hartree-Fock component but can be a local and/or gradient corrected functional. Conceptually the hybrid exchange and correlation functional is defined:

$$E^{XC}_{hybrid}=c_{HF}E^{X}_{HF}+c_{DFT}E^{XC}_{DFT} \qquad 4.2$$

Where c's are constants

E^{XC}_{hybrid} is the exchange and correlation term for a hybrid functional

E^{X}_{HF} is the exchange term for Hartree Fock

E^{XC}_{DFT} is the exchange and correlation term for DFT [Foresman, 1993]

One very popular hybrid functional is called Becke, 3-parameter, Lee–Yang–Parr or B3LYP for short. B3LYP is a global hybrid functional. Global hybrid functionals use a constant percentage of exact Hartree-Fock exchange for both short and long range. As seen in Table 4.1, B3LYP uses a constant 20% Hartree-Fock exchange [Avhad, 2017; Paier, 2007]. Although B3LYP is the most popular hybrid functional, it is a global hybrid and is not long range corrected. Therefore, B3LYP significantly underestimates charge transfer excitations [Bhatta, 2015; Korzdorfer, 2011; Avhad, 2017; Borpuzari, 2017; Yanai, 2004; Refaely-Abramson, 2011; Chai, 2008; Sekar, 2018; Pandey, 2012].

4.3 Range-Separated Functionals

Global hybrid functionals use a constant amount of exact (Hartree-Fock) exchange for both short and long range [Avhad, 2017]. Global hybrid (GH) functionals are not long range correct (LC), therefore they underestimate charge transfer excitations. The underlying cause is of these errors occurring with global hybrid functionals is the delocalization or self-interaction error. For charge transfer, long range corrected DFT (LC-DFT) is needed. The success of LC-DFT in describing acceptable excited state phenomena is due to the required fraction of Hartree-Fock exchange incorporated with increasing inter-electronic distance. The range separated hybrid (RS) functionals used in LC-DFT separate the exchange energy (E_X) into short range (SR) and long range (LR) contributions. RS functionals include the exact HF exchange for the long-range interaction and employ the local DFT exchange for the short-range interaction. The DFT exchange interaction is included using the first term which is for short range and the long range orbital-orbital exchange interaction is described with the Hartree-Fock (HF) exchange integral in the second term [Yanai, 2004].

$$E_X^{LC\text{-}DFT} = E_X^{SR\text{-}DFT} + E_X^{LR\text{-}HF} \quad 4.3$$

$E_X^{LC\text{-}DFT}$ is the exchange term for long range corrected DFT

$E_X^{SR\text{-}DFT}$ is the exchange energy using DFT in the short range

$E_X^{LR\text{-}DFT}$ is the exchange energy using Hartree Fock in the long range

This separation is achieved by bifurcating the interelectronic Coulomb operator r_{12}^{-1}

$$\frac{1}{r_{12}} = \frac{1-efr(\omega r_{12})}{r_{12}^{SR}} + \frac{\mathrm{erf}\,(\omega r_{12})}{r_{12}^{LR}} \quad 4.4$$

Here erf is defined as the inaccuracy function and ω is defined as the range separation parameter [Sekar,2018]. $1/\omega$ defines a characteristic length scale for transition between the SR and LR descriptions. $1/2\omega$ corresponds to the distance at which the Coulomb operator transitions from being treated mostly by the SR description to being treated mostly by the LR description [Korzdorfer, 2011]. Range-separated hybrid functionals solve problems with DFT including chain length dependence on ionization potentials, excitation energies, and orbital energies of conjugated systems. [Bhatta, 2015; Korzdorfer, 2011; Avhad, 2017; Borpuzari, 2017; Yanai, 2004; Refaely-Abramson, 2011; Chai, 2008; Sekar, 2018; Pandey, 2012]. Both CAM-B3LYP and wB97XD are range-separated hybrid functionals and both are considered good functionals for determining excitation energies. CAM-B3LYP is a Coulomb attenuated version of B3LYP comprised of 19% Hartree-Fock exchange interaction at short range and 65% Hartree-Fock at long range. The intermediate region is smoothly described through a standard error function with a default range separation parameter value of ω = 0.33 [Yanai, 2004]. wB97XD is a range-separated version of Becke's 97 functional with additional dispersion correction. WB97XD

is comprised of 22% Hartree-Fock exchange at the short range and 100% Hartree-Fock at the long range. The intermediate region is smoothly described through a standard error function with a default range separation parameter value of ω = 0.2 [Chai, 2008]. (Table 4.1)

Table 4.1: % Hartree-Fock exchange composition in GH and RS Functionals [Avhad, 2017]

Functional	Default ω value	Global Hybrid(GH) or Range Separated Hybrid (RSH)	Hartree-Fock % Short Range/Long Range
B3LYP	N/A	GH	20
CAM-B3LYP	0.33	RS	19/65
wB97XD	0.2	RS	22/100

Range-separated hybrid functionals are important for orbital energy modeling of conjugated molecules that involve charge transfer excitation. The computed results accuracy, however, depend on the range-separation parameter ω. Previous research by Bhatta [Bhatta, 2015] indicates that the values for ω that produce accurate orbital energies in conjugated systems are much lower that the default values for CAM-B3lyp (ω=0.33) and wb97xd (ω=.2). They found that the best values for ω are between 0.1 and 0.15 $Bohr^{-1}$. One goal of the work reported here was to determine the most accurate range separation parameter values for modeling MEH-PPV of various chain lengths as well as investigating the effect of different solvents.

4.4 Basis sets

In addition to specifying a functional, one must also specify a basis set when using Gaussian software. Linear combinations of gaussian functions form the orbitals for standard basis sets. Larger basis sets approximate the orbitals more accurately because they impose fewer restrictions on the locations of the electrons in space. As polarization and diffuse functions are added, the result of the calculation becomes more accurate. Table 4.2 summarizes a series of available basis sets.

Table 4.2. Basis sets in Gaussian

Basis Set	Properties
6-31G	Standard Split valence basis.
6-31G(d)	also known as 6-31G*: Adds polarization functions to heavy atoms
6-31+G(d)	Adds diffuse functions
6-31++G(d,p)	Adds polarization and diffuse functions to hydrogens
6-311+G(d)	Adds extra valence functions to 6-31+G(d)
6-311++G(d,p)	Adds polarization and diffuse functions to hydrogens in 6-311+G(d) (GB)

This series begins with a split valence basis set. The first way that a basis set can be made larger is to increase the number of basis sets per atom. A split valence basis set has two (or more) sizes of basis function for each valence orbital. This series of basis sets listed starts with this split valence and successively adds basis functions to heavy atoms, then hydrogens, then increases the number of valence level basis functions and repeats adding expansions on heavy atoms and hydrogens. In general, improving polarization and adding

diffuse functions both lead to more accurate calculations, however, for large molecules, the increased complexity may result in unacceptable computational cost.

4.5 Polarizable Continuum Model

Unless otherwise noted, all of the experiments reported in this work were MEH-PPV in solution. In order to take the solvent into account theoretically, the Polarizable Continuum Model (PCM) was used. The Polarizable Continuum Model (PCM) is a commonly used method in computational chemistry in which the solvent molecules are treated implicitly instead of explicitly and the molecular free energy of solvation is computed as the summation of three terms; free energy for electrostatic interaction, dispersion-repulsion, and cavitation [Giri,2014]. Our theoretical work matched our experimental work by using dilute solutions of MEH-PPV in five different solvents.

Chapter 5

Initial modeling MEH-PPV polymer

5.1 Effect of increasing chain length

Initial modeling was performed using DFT and the Global Hybrid functional Becke three parameter Lee-Yang-Parr otherwise known as B3LYP. The basis set used in this early work was 6-31G, the standard split valence basis described in chapter 4.

The effect of increasing the chain length of the MEH-PPV polymer on the shift of the photo absorption peak was studied by considering different MEH-PPV polymer units beginning with a monomer and increasing to a decamer. The structures of these oligomers were first optimized in the gas phase using density functional theory. The dynamical stabilty of all ground state geometries was confirmed by calculating their normal mode frequencies which were all positive. The UV-VIS spectra were calculated using time dependent density functional theory [Bauernschmitt, 1996; Scalmani, 2006] (TD-DFT) and gas phase optimized geometries. The electrospinning experimental UV-VIS study (described in Chapter 3) was carried out using chloroform as a solvent, therefore the UV-VIS spectra in choloroform was calculated by employing PCM [Tomasi, 2005] approach within the TD-DFT methodology. To investigate the influence of bond stretching in the polymer chains, the double bonds linking the monomers in the polymer were gradually stretched from their equilibrium distance to higher bond lengths. The UV-VIS calculations were performed in

both gas and solvent phase. All calculations were carried out using Gaussian03W suite of programs [Frisch, 2003].

The equilibrium geometry of a monomer unit of MEH-PPV was first optimized resulting in the structure given in Fig. 2.2. The structures were optimized as successive monomer units were added to form an oligomer containing up to 10 monomers. The geometry of the pentamer is shown in Fig. 5.1. The geometry of the individual monomer units remain essentially unchanged as the chain length is increased. For each of the oligomers starting from monomer to decamer, the UV-VIS spectra was calculated. The results are plotted in Fig. 5.2 (a). A red shift in the absorption spectra can be seen as the length of the polymer increases. This is because increasing number of monomer units in the polymer increases the effective π conjugation length which in turns leads to smaller HOMO-LUMO gap (see Fig. 5.2(b)). With increase in π conjugation length, the energy required to excite an electron decreases, and consequently the wavelength that provides this energy increases [Giri, 2014].

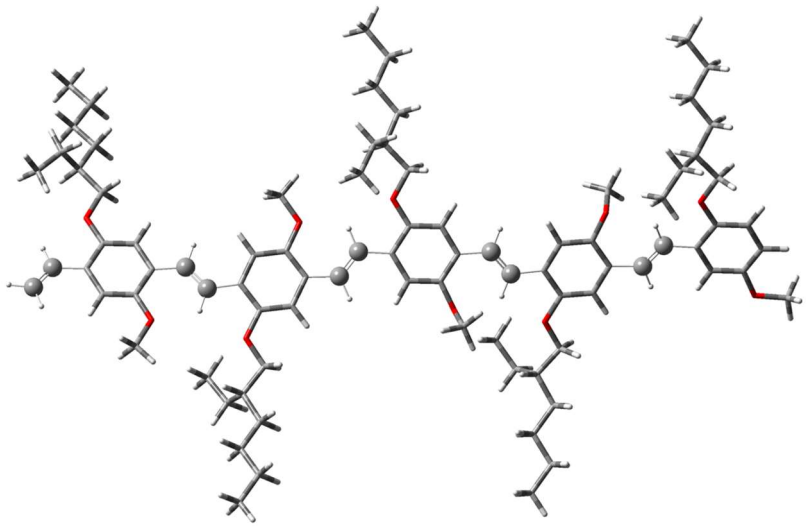

Figure 5.1: Optimized Geometry of MEH-PPV pentamer. Grey Spheres represent Carbon atom linking monomer units

This results in bathochromic shift in the absorption spectrum which is consistent with a decrease in HOMO-LUMO gap as the polymer length increases.

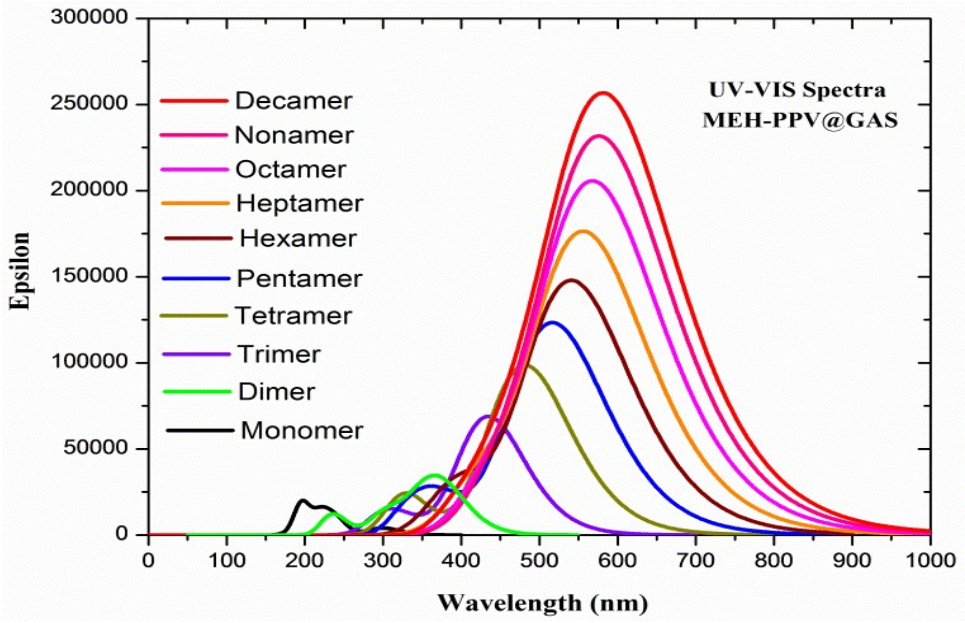

(a)

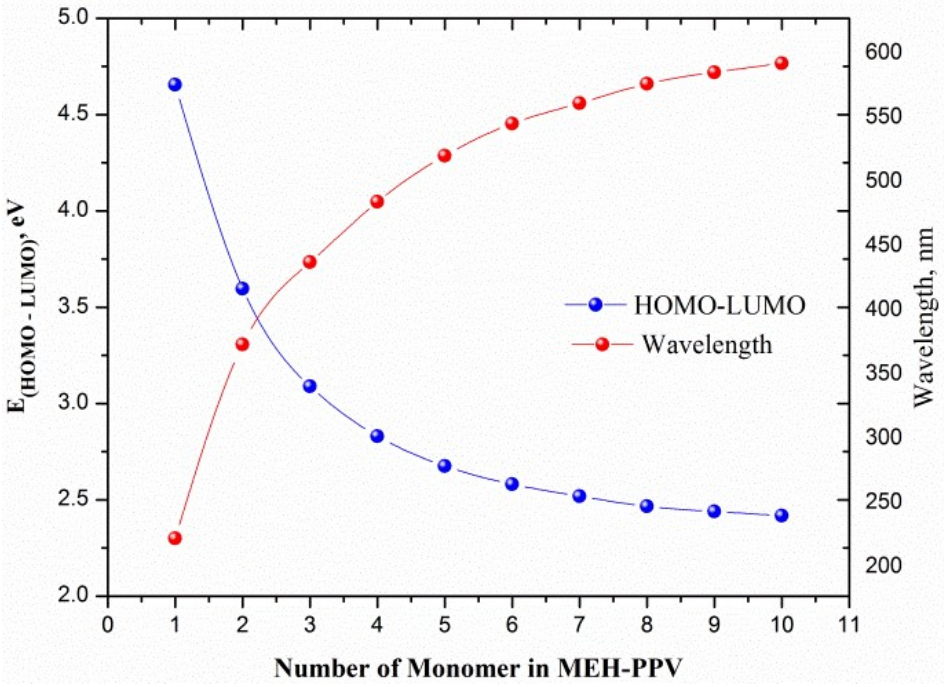

(b)

Figure 5.2: Theoretically calculated UV-VIS spectra (a) and HOMO-LUMO gap with wavelength (b) for different chain length of MEH-PPV polymer [Giri, 2014]

5.2 Impact of stretching C=C linkage bonds

During electrospinning an electrical charge is used to pull the polymer to form a very fine fiber. It is likely that this process could stretch the inter-atomic bonds in the polymer. To investigate the effect of this stretching on the UV-VIS spectra, work was done that focused on the most likely bond that can stretch, namely the C=C double bond linking the monomers. Determining an appropriate length of monomer chain necessary to reproduce the photo absorption peaks of the MEH-PPV polymer was necessary. In other words, it was necessary to determine when the wavelengths saturate. The results are plotted in Fig. 5.3. Note that the peak wavelength in the absorption spectrum increases rapidly from monomer to pentamer and begins to saturate [Giri, 2014]. Therefore, for the study of stretching of the linkage bonds we used the pentamer to model the MEH-PPV polymer. Absorption is actually controlled by the conjugation length of the chromophores and not the chain length. Increasing the chain length does not necessarily affect the conjugation length of the chromophores within the conjugated backbone but the conjugation length cannot exceed the chain length [Traiphol, 2010]. Although conjugation lengths ranging from two to twelve monomer units have been reported [Kasha, 1963;Yamagata,2014], the choice of five monomer units for our theoretical model of an MEH-PPV polymer chain was confirmed by Kohler, Hoffman and Bassler. They reported that at room temperature MEH-PPV chains have effective conjugation lengths of about five repeat units [Kohler, 2012]. For this reason, a pentamer was used for the initial theoretical model of an MEH-PPV polymer chain.

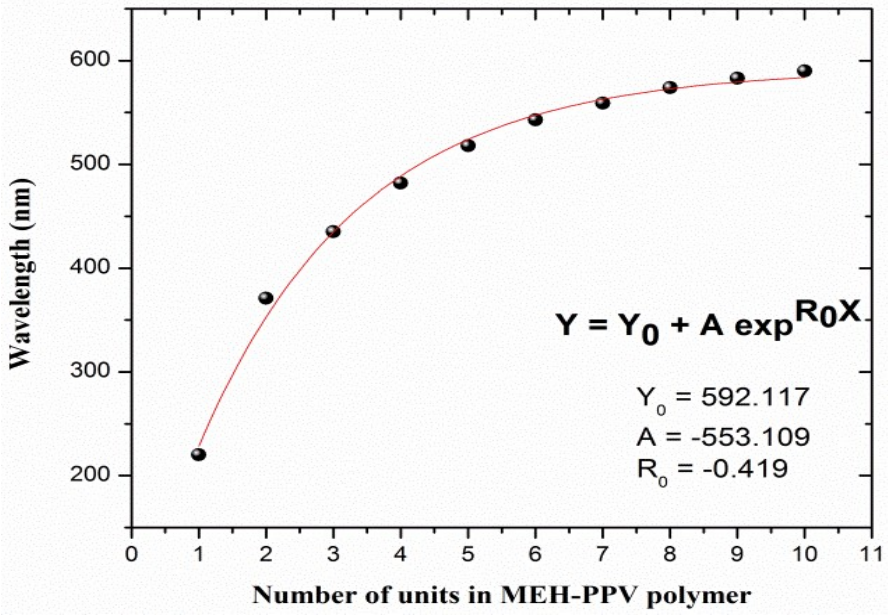

Figure 5.3: Exponential plot for wavelength corresponding to the absorption peak vs. number of monomer units forming the MEH-PPV polymer.

Several UV-VIS spectra for a pentamer were calculated as incremental changes in the double bonds increased from 1.36 to 1.45 Å. It was found that the linkage transforms from a double bond (1.36-1.38Å) to a partial double bond (1.39-1.42 Å), and eventually to a single bond for at 1.45 Å. The calculation first performed in the gas phase was repeated in the solution phase with the chloroform solvent. The results are illustrated in Figures 5.4 (a), (b) and (c). Figure 5.4(a) shows theoretical results performed in the gas phase while Figure 5.4(b) corresponds to the result in the chloroform solution [Giri 2014]. In both cases a red shift occurs as the linking bond is stretched. Because of the solvent effect, the spectra in chloroform are shifted further to the red than that in the gas phase. These results agree well with the experimental observation and show that solvent, bond stretching, and increasing chain length all contribute to the observed red shift in the electrospun fiber.

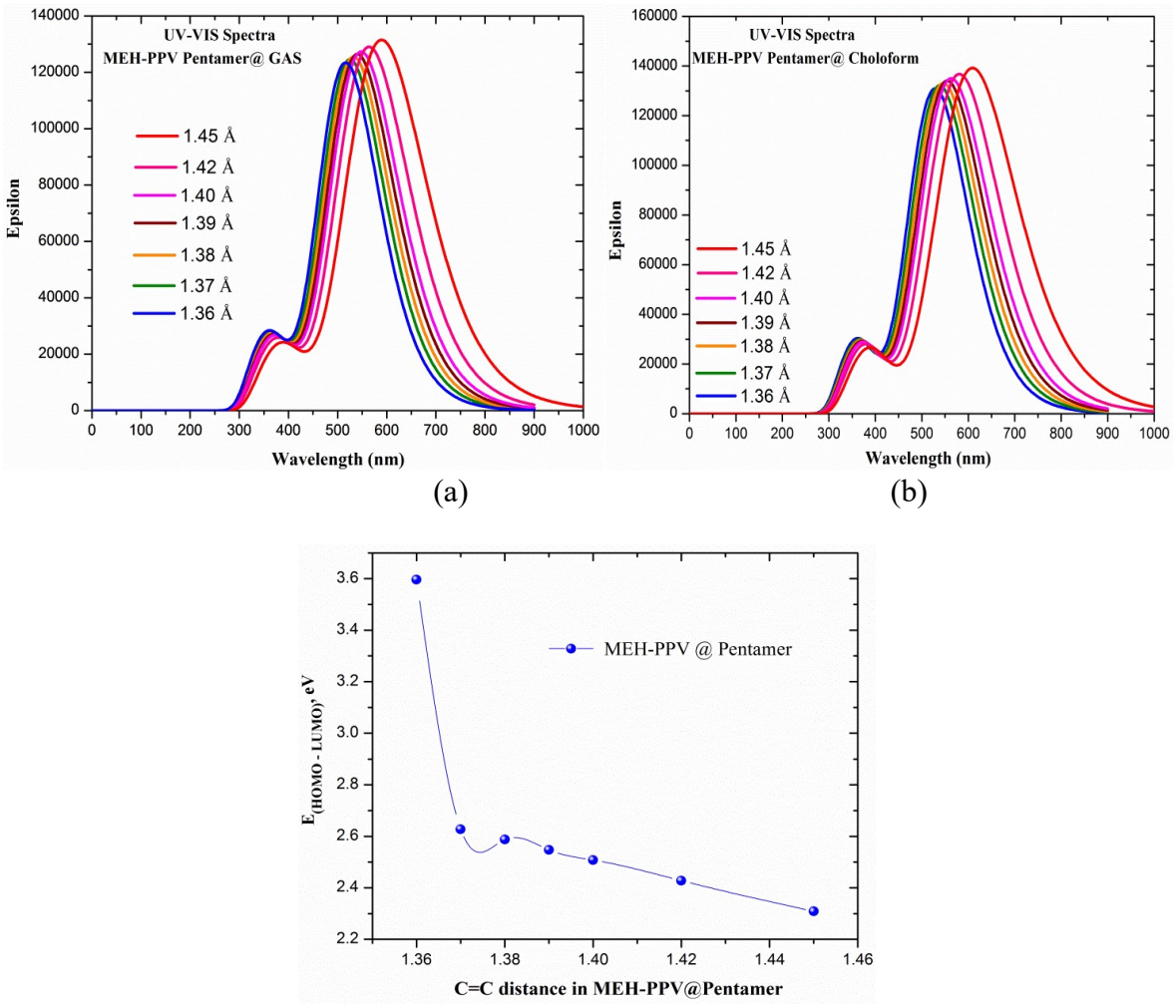

Figure 5.4: Variation of UV-VIS Spectra in gas (a), solvent (b) and HOMO-LUMO gap (c) for diffferent C=C distance in MEH-PPV pentamer. [Giri,2014]

To investigate the reason behind the red shift with increase in C=C linkage distance we have calculated the HOMO-LUMO gap for different distances. The corresponding plot is given in Figure 5.4(c). We note that the HOMO-LUMO gap indeed decreases with increasing C=C distance causing the redshift in the spectra [Giri,2014].

We compare our early computational results to experimental results obtained by Tilley et al in Table 5.1. While our computational results follow the same trend as found in experiment, the actual results are significantly different.

Table 5.1: Comparison of UV-VIS wavelength between theory and experiment [Tilley, 2011]

Number of monomer in MEH-PPV	**UV-VIS wave length (nm)**	
	Experiment(14)	**Theory**
3	397	435
4	431	482
5	451	518

The trend of lengthening oligomer corresponding to a red-shifted UV-Vis peak absorption is seen in both the experimental and theoretical values. The theoretical values are all significantly higher than the experimental values, and the gap between the theoretical and experimental increases with increasing chain length. The difference for trimer is 38 nm, for tetramer is 51 nm, and for pentamer is 67 nm. For this portion of the study density functional theory with the B3LYP functional [Giri, 2014] to account for exchange-correlation contribution to potential was used. As discussed in Chapter 4, B3LYP is a global hybrid functional that is not long range corrected and significantly underestimates charge transfer excitations [Bhatta, 2015; Korzdorfer, 2011; Avhad, 2017; Borpuzari, 2017; Yanai, 2004; Refaely-Abranson, 2011; Chai, 2008; Sekar, 2018; Pandey, 2012].

In order to create models whose magnitudes agree with the experimental values versus just agreeing with the trends of the experimental values, in later work long range corrected functionals and a basis set that includes polarization functions were used. As discussed in Chapter 4, range separated hybrid (RS) functionals separate the exchange

energy (E_X) into short range (SR) and long range (LR) contributions. RS functionals include the exact HF exchange for the long-range interaction and employ the local DFT exchange for the short-range interaction. Range separated functionals are much more accurate than global hybrid functionals when estimating charge transfer excitations. In addition to changing the functional and the basis set, the range separation parameter was the key to creating models that agree with experimental values. Chapter 7 gives further detail regarding this advanced modeling of MEH-PPV.

Chapter 6

Impact of Interchain and Intrachain interactions on absorption

6.1 Morphology/ Chain Conformation

The performance of conjugated polymer solar cells depends on morphology [Chiu, 2012]. The morphology of MEH-PPV chains in solution has a great influence on absorption [Nguyen, 1999; Traiphol, 2010; Spano, 2014]. Specifically, the morphology of polymer chains refers to their form and structure and two aspects of morphology are chain conformation and aggregation. Chain conformation refers to the structural arrangement of the chains and aggregation refers to direct mutual attraction of the molecules. Both the physical conformation of the polymer chains and the way they pack together (aggregation) determine many of the important optical and electronic properties that are critical to the operation of devices based on these materials [Schwartz, 2003].

The morphology of polymer chains in solution depends on both the solvent used and the polymer concentration [Schwartz, 2003; Nguyean, 1999; Traiphol, 2010; Quan, 2006]. Different solvents can change the morphology of the polymer chain. The variation of local polymer-solvent interactions forces the MEH-PPV chain to adopt different conformations in the solvents. In a "good" solvent, where polymer backbone-solvent interactions are favorable, the MEH-PPV chain will adopt an open, extended conformation. In a "poor" solvent, polymer backbone-solvent interactions are not favorable and the polymer twists and

coils to avoid these interactions. Figure 6.1 illustrates the effects of good and poor solvents. Conjugation lengths of MEH-PPV decrease when the extended chain is forced to collapse in a poor solvent. This twisting and coiling in a poor solvent can break the conjugation length of the polymer chain, causing shorter conjugation lengths [Schwartz, 2003; Nguyen, 1999; Traiphol, 2010]. Randomly appearing torsion angles between adjacent monomer units effectively interfere with the behavior of the π electron so that conjugation length is much shorter than the physical length of the whole polymer [Chang, 2000]. Morphology has a great influence on conjugation lengths of the polymer chains which in turn has a great influence on absorption [Traiphol, 2010; Lampert, 2014]. Longer conjugation lengths cause the absorption spectrum to red shift [Nguyen, 1999; Traiphol, 2010; Collison, 2001; Zhu, 2009]. Because of these effects, understanding solvent effects on absorption could make polymer solar cells more efficient.

Figure 6.1 is a schematic representation of what happens with the morphology of polymer chains in good and poor solvents. In poor (nonaromatic) solvents, the polymer chains coil tightly to maximize solvent-side-group interactions and to minimize exposure of the aromatic backbone to the solvent. In good (aromatic) solvents, the aromatic backbone of the polymer chain adopts a rigid, open conformation in solution. With the backbone open and exposed, it is straight forward for the π-electron on one chain to overlap with the neighboring chain [Zayana, 2013]. This is known as π-π stacking in interchain aggregation. This aggregation causes a red shift in the absorption spectrum. Aggregation is discussed more in Sec. 6.2. Collapsed chains caused from a poor solvent can cause breaks in the conjugation lengths and therefore a blue shift from the previously longer conjugation lengths. If the chains do not have an open conformation it is difficult for the π-electrons to

overlap and it is difficult for aggregation to take place. In this case agglomerates instead of aggregates are formed. Agglomerates do not interact electronically and the absorption spectrum is unchanged from the absorption spectrum of isolated chains.

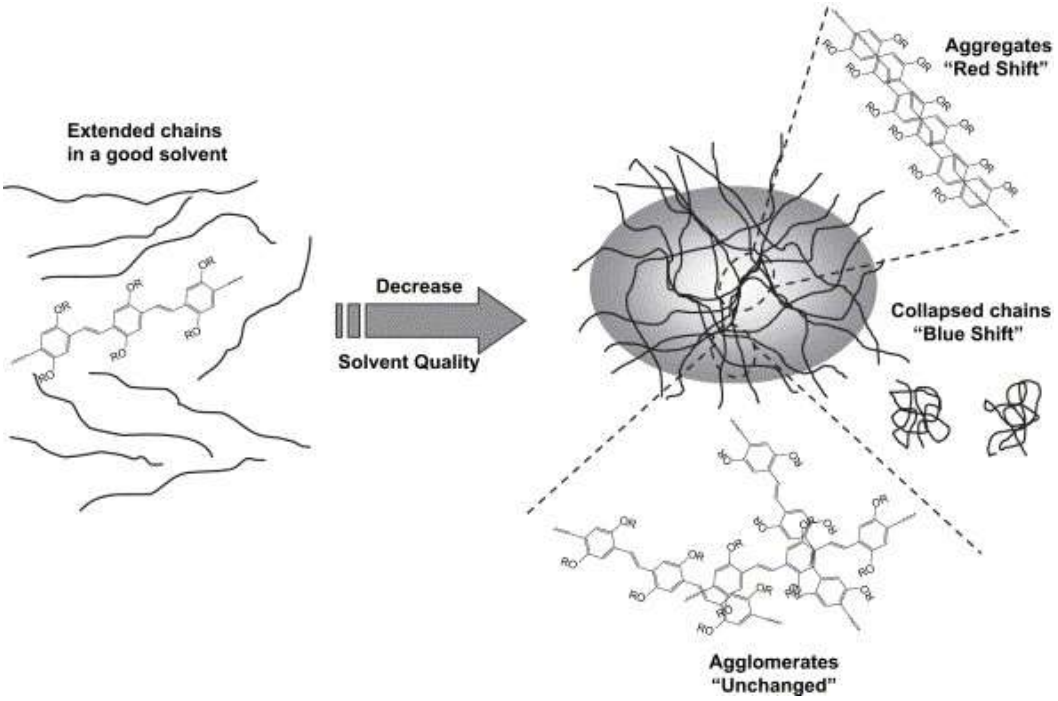

Figure 6.1: Schematic representation of polymer morphology in good and poor solvents [Traiphol, 2007]

6.2 Aggregation

In order to study morphology, one must study aggregation. Aggregates of conjugated polymers exhibit two classes of fundamental electronic interactions. Intrachain interactions occur within a given chain and Interchain interactions occur between chains. Both intrachain and interchain couplings result from aggregation [Yamagata, 2012]. The impact of these excitonic interactions on the photophysics of polymer films can be

understood using the concepts of J- and H- aggregation. This concept was originally developed by Kasha and his group [Kasha, 1963; Hochstrasser, 1964] to treat aggregates of small molecules. In polymers, intrachain through-bond interactions lead to J-aggregates behavior and interchain Coulombic interactions lead to H-aggregate behavior. Single chains of emissive conjugated polymers behave photophysically like J-aggregates. The photophysics of conjugated polymer π stacks is determined by a competition between J-favoring intrachain interactions and H-favoring interchain interactions [Spano, 2014]. The morphology of the polymer chains in solutions determines how the chain packing of the H-type aggregation can be performed. Open coil conformation that occurs in good solvents tends to promote interchain aggregation as compared to poor solvents that make a compact conformation of tightly coiled chains that resist interchain aggregation.

The competition between interchain and intrachain interactions has been observed in many studies, but there is not agreement on how much each type of aggregation is contributing. The π stacking that happens in MEH-PPV solution thin films and solutions must be treated as both interchain and intrachain coupling. In other words, polymer π stacks are inherently 2D excitonic systems with electronic excitations delocalized along the polymer backbone as well as between the chains [Spano, 2014]. Numerous experiments have been performed on a variety of conjugated polymers and the results of these studies have estimated the fraction of photoexcitations that result from interchain species ranges from 90% to essentially 0% [Schwartz, 2003].

In section 6.1 the fact that randomly appearing torsion angles in the polymer backbone interfere with the intrachain behavior of the π electron moving along the backbone

and shorten the conjugation length [Chang, 2000] was discussed. Longer conjugation lengths promote better intrachain interactions and a red shift in the absorption spectrum. Longer conjugation lengths are possible with open conformation of the polymer chains. Better chain packing will also result from the open conformation of chains and thus, in interchain interactions. Strong interchain interactions favor charge transport. Maximum chain overlap would be optimal for photovoltaic devices that require high charge transport and minimal luminescence efficiency [Schwartz, 2003].

Figure 6.2 illustrates a single PPV polymer chain and its potential morphology. Figure 6.1 shows the differences in the extended, open chain conformation of a good solvent and tightly coiled conformation of a poor solvent. The twisting of the polymer chain and the breaking of the conjugation length is also illustrated (conjugation length was discussed in section 5.1). Finally, interchain interactions made possible from aggregation and intrachain interactions along the polymer backbone are also illustrated. (Although this is an illustration of a single polymer chain, interchain interactions typically come from 2 separate polymer chains π-π stacking and forming interchain aggregates) [Spano, 2014].

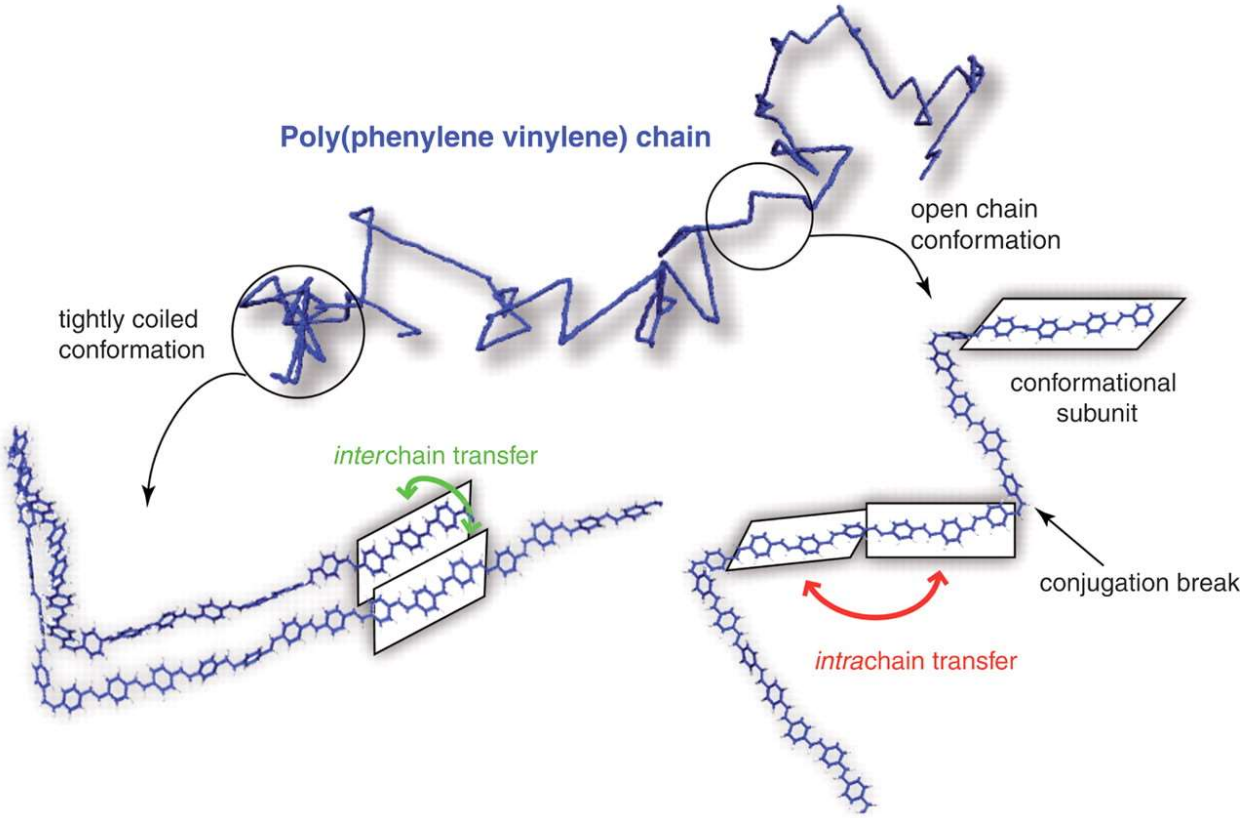

Figure 6.2: Example of single-chain conformation of poly(phenylene) conjugated polymer. [Collini, 2009]

6.3 "Memory" of Morphology

The optical and electronic properties of conjugated polymers are sensitive to the polymer morphology in the solution-cast thin films used in most applications. Morphology of thin films in turn depends on the polymer conformations in the solution phase [Chiu, 2012]. Evidence suggests that "memory" of the solution-phase conformation of MEH-PPV is retained through the spin-casting process of making a thin film. This results in solution-phase control over the morphology and photophysics of conjugated polymer films. This is observed in studies of samples that used the same spin-casting technique but used different

solvents in an MEH-PPV solution. These samples had different degrees of interchain coupling. The photophysics of MEH-PPV in films cast from different solvents have different photophysical properties [Nguyen, 1999][15]. Both X-Ray [Schwartz, 2003; Yang, 1998] and electron diffraction[Schwartz, 2003; Weir,1999] studies indicate differences in the chain packing results of aggregation in MEH-PPV films cast from different solvents. “Memory” of the chain conformation in solution somehow persists through the spin-casting process, producing films with different underlying chain packing morphologies. Memory of the solution chain conformation and coil shape is also carried through the spin-coating process and endures into the film [Schwartz, 2003].

6.4 Pentamer

In an effort to study interchain and intrachain interactions, an MEH-PPV pentamer was first optimized in the gas phase using the Becke three parameter Lee-Yang-Parr (B3LYP) form for the exchange-correlation potential and a 6-31G basis set. The pentamer was chosen based on previous work which demonstrated that a pentamer is a good polymer chain length for modelling purposes [Giri 2014]. Although conjugation lengths ranging from two to twelve monomer units have been reported [Kasha, 1963; Yamagata, 2014], the choice of five monomer units for our theoretical model of an MEH-PPV polymer chain was confirmed by Kohler, Hoffman and Bassler [Kohler, 2012]. They reported that at room temperature MEH-PPV chains have effective conjugation lengths of about five repeat units. Figure 2.2 shows the model of the MEH-PPV pentamer optimized in the gas phase as illustrated in Gauss-view software. The section below models of a pair of stacked pentamers in which interchain interactions could occur between the pentamers.

6.5 Stacked Pentamers

Chain morphology depends on the solvent used and the polymer concentration. With the PCM model in Gaussian, the basic calculation is performed on a single molecule with a continuum model for the solvent. This is effectively a calculation corresponding to infinite dilution. The experimental numbers are based on a 0.002 weight percent solution, but even this highly diluted experimental solution does not yield a single molecule in an infinitely dilute solution. To better understand how concentration affects the theoretical results, two pentamers were stacked on each other and optimized in the gas phase in Gaussian 09. The gas phase optimized stacked pentamer model as illustrated by Gauss-view software is seen in Figure 6.3. When more than one chain is stacked, the result is π-π stacking and aggregation. Polymer chains tend to aggregate with increasing concentration. The degree of aggregation is both concentration and solvent dependent [Huo, 2011]. Studying the π-π stack gives us an idea of how aggregation affects the UV-Vis spectrum.

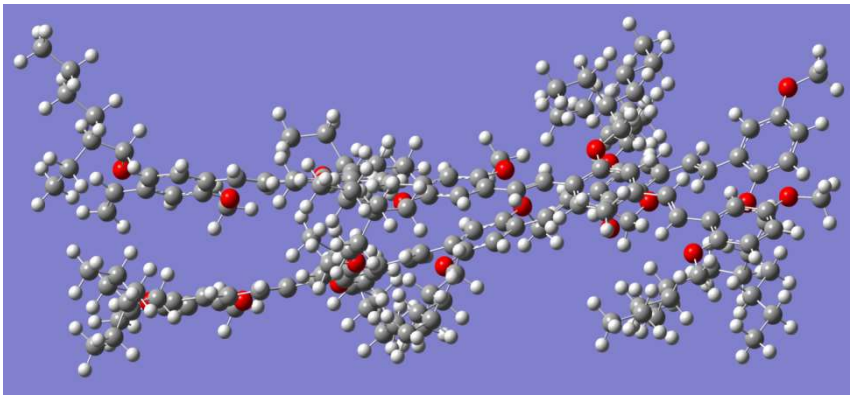

Figure 6.3: Optimized geometry of two stacked MEH-PPV pentamers

The UV-Vis peak absorptions for the stacked pentamer model in each solvent were obtained theoretically using Gaussian 09 quantum chemistry software. As with the single pentamer model, the structure of the stacked pentamer model was optimized in the gas phase using B3LYP for the exchange-correlation potential and 6-31G as the basis set. The gas phase model was then re-optimized in all five solvents by using B3LYP and the same basis set in combination with the Polarizable Continuum Model (PCM). PCM within Time Dependent Density Functional Theory (TD-DFT) was then used to calculate the UV-Vis spectra of MEH-PPV in solution.

6.6 Decamer

In order to compare inter-chain and intra-chain transfer, a decamer (polymer chain consisting of 10 monomers) was modeled in the Gauss-view software. The stacked pentamers include 10 monomer units just as the decamer includes 10 monomer units. The stacked pentamers model allows for inter-chain aggregation because the overlap of the molecules provides the opportunity for π-π stacking of polymer chains that would allow inter-chain transfer. The decamer model allows only for intra-chain transfer along the polymer chain.

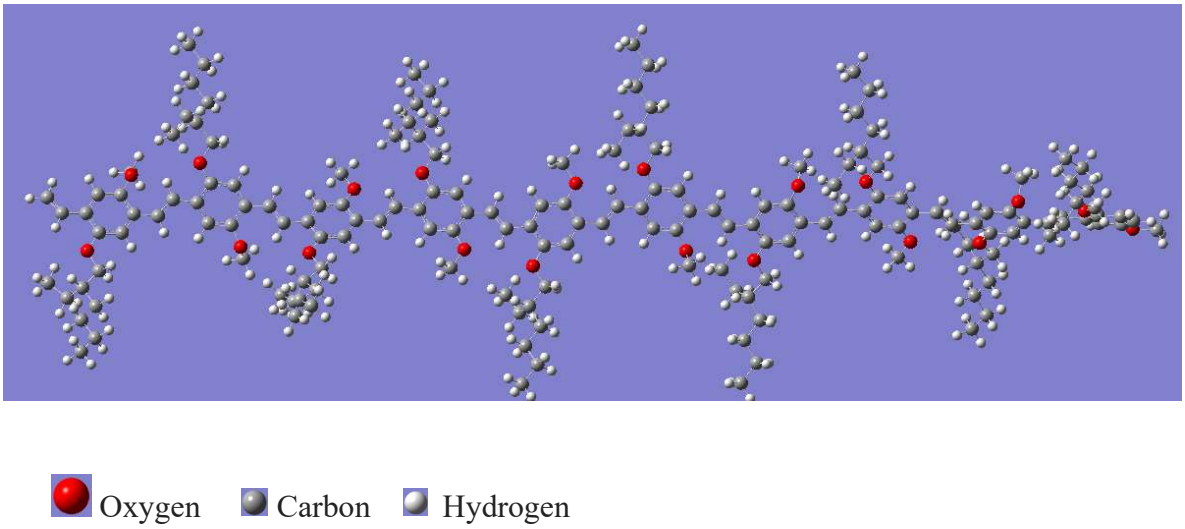

Figure 6.4: Optimized geometry of an MEH-PPV decamer

Like the single pentamer and the stacked pentamer models, the decamer was optimized in the gas phase using B3LYP for the exchange-correlation potential and 6-31G as the basis set. The optimized decamer model, as illustrated by Gauss-view software, is seen in Figure 6.4. The gas phase model was then re-optimized in all five solvents by using B3LYP and the same basis set in combination with the Polarizable Continuum Model (PCM). PCM within Time Dependent Density Functional Theory (TD-DFT) was then used to calculate the UV-Vis spectra of MEH-PPV in solution.

Table 6.1 lists the wavelengths corresponding to the absorption peaks for MEH-PPV measured experimentally and modeled theoretically as a single pentamer, a stacked pentamer, and a decamer.

Table 6.1: Wavelength corresponding to Absorption Peak (nm) (Theoretical data from model of single pentamer, model of two stacked MEH-PPV pentamers, and MEH-PPV decamer)

	Experiment (nm)	Single Pentamer Theory (nm)	Stacked Pentamer Theory (nm)	Decamer Theory (nm)
Gas		517.89	538.08	590.42
Chloroform	496	534.19	544.66	597.95
Toluene	501	535.25	545.43	599.84
Xylene	501	535.32	545.47	600.38
Dichloromethane	502	534.05	548.65	599.18
Chlorobenzene	505	535.96	549.89	599.42

To help in understanding the data in Table 6.1, Figs. 6.5 and 6.6 have been plotted. Figure 6.5 shows the correlation of the absorption peaks between the experimental data, the (normalized) theoretical stacked pentamer data, and the (normalized) theoretical decamer data. Each data point in the stacked pentamer data has been reduced by 44 nm to facilitate the comparison with the experimental data. Similarly, each data point in the decamer data has been reduced by 93 nm to facilitate the data comparison.

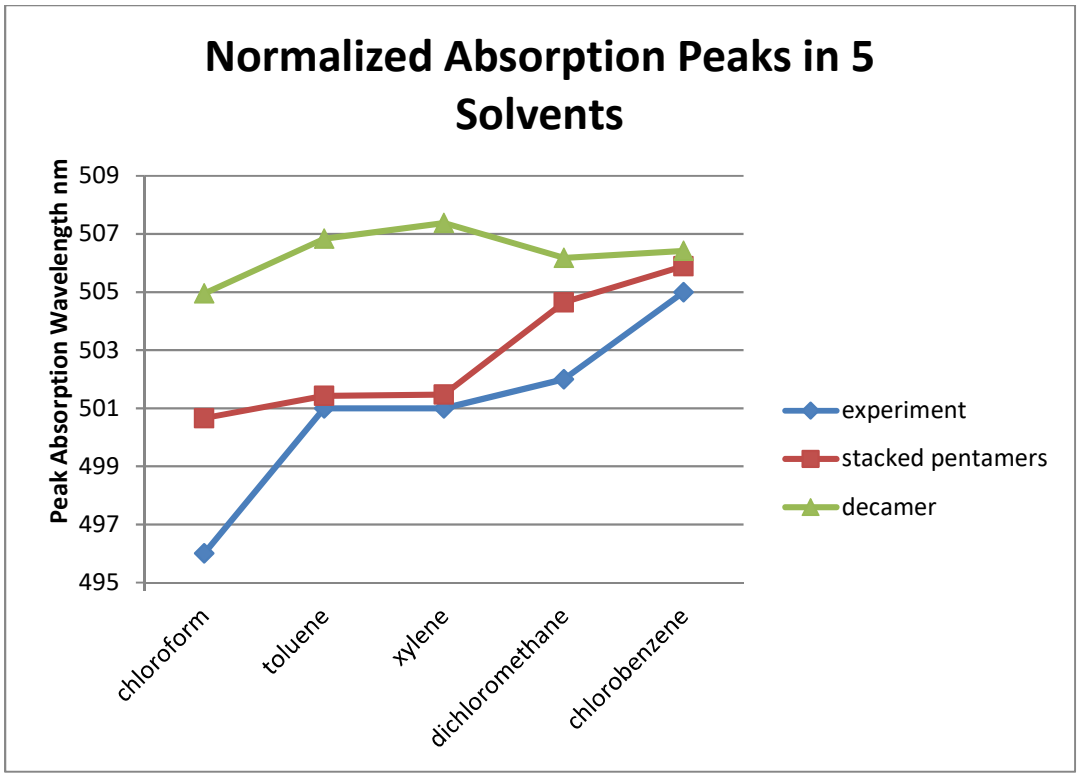

Figure 6.5: Correlation between experimental data, normalized theoretical stacked pentamer peak wavelength (nm) (reduced by 44 nm for ease in comparison), and normalized theoretical decamer peak wavelength (nm) (reduced by 93 nm for ease of comparison).

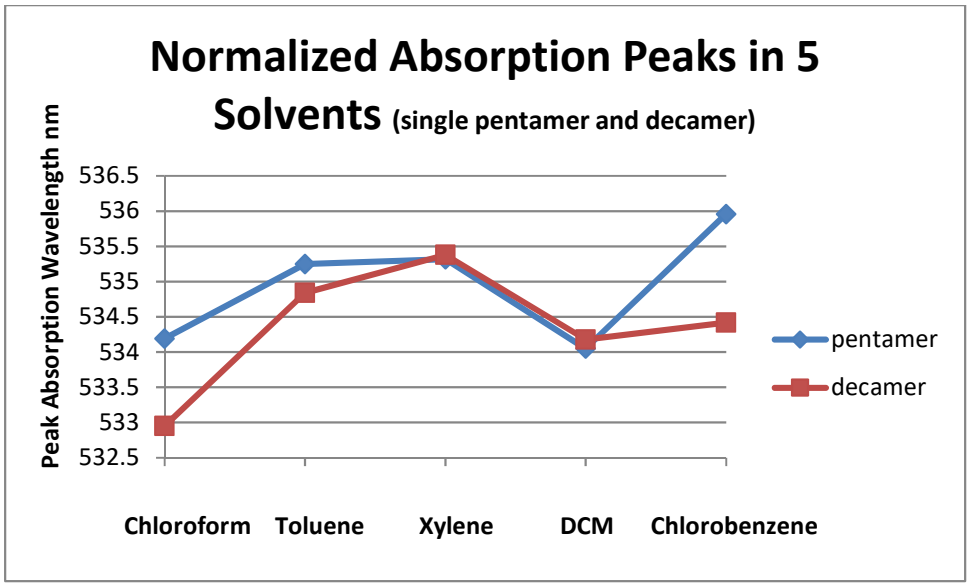

Figure 6.6: Correlation between the theoretical single pentamer and the (normalized) theoretical decamer wavelength (nm) (reduced by 65 nm for ease of comparison) corresponding to absorption peak

As can be seen from Figs. 6.5 and 6.6, the magnitudes of the red shifts in the absorption peaks calculated using the stacked pentamer model for each solvent correlate closely with those measured experimentally. Similarly, red shifts in the absorption peaks calculated using the single pentamer model and the single decamer model correlate well. However, the single pentamer and decamer models do not correlate well with the experimental results.

As can be seen from Fig. 6.5, the absorption peaks calculated using the stacked pentamer model for each solvent correlate better overall with the experimental data than the values from the decamer model. The values for the stacked pentamer model correlate very closely with the values measured experimentally for the aromatic solvents (chlorobenzene, toluene, and xylene). Red shifts in the absorption peaks calculated using the single

decamer model do not correlate well with the experimental data, but the non-aromatic solvents (chloroform and dichloromethane) show dips in the theoretical decamer graph that resemble dips seen experimentally with the aromatic solvents. This leads to the belief that the aromatic solvents behave more like the stacked pentamers and the non-aromatic solvents behave more like a single polymer chain. This makes sense because "good" (aromatic) solvents promote open chain conformation and enable pi-pi stacking, while poor solvents twist and curl and do not enable pi-pi stacking. Studies by Traiphol et al and Lampert et al found the degree of aggregation was higher in the aromatic solvent chlorobenzene in which MEH-PPV adopts an open coil conformation when compared to the non-aromatic solvent tetrahydrofuran [Traiphol,2010] [Lampert, 2014]. Aggregation between MEH-PPV chains in dilute solutions is promoted when the backbone is straight and hindered when the backbone is coiled [Schwartz, 2003]. This leads us to believe that aromatic solvents promote interchain aggregation and non-aromatic solvents limit interchain aggregate formation. The aromatic solvents interact with the polymer backbone and promote an open chain that allows interchain aggregation between polymer chains whereas the non-aromatic solvents interact with the polymer side chains and promote twisting of the polymer chain.

The close correlation between the experimental and the theoretical stacked pentamer data can be understood from several perspectives. First, the theoretical single pentamer and decamer models are performed as infinitely dilute solutions. Any experimental solution for which the absorption can be measured will have a non-zero concentration and thus interaction between separate polymer chains. The stacked pentamer model simulates this behavior and therefore provides a better correlation to the experimental data. This provides evidence that inter-chain interactions play an important role in absorption red-shift.

Second, it is necessary to look at the "quality" of the solvents. In an "infinitely dilute solution" (simulated by the single pentamer and decamer models), solvent quality will play a different role as there is no inter-chain interaction possible. It will, however, influence how the polymer chain will coil back on itself. Figure 6.6 compares the single pentamer (5 monomers) data and the single decamer (10 monomers) data. For both of the single chain models (pentamer and decamer), the aromatic solvents (particularly toluene and xylene and to some extent chlorobenzene) show an absorption peak that is red-shifted relative to the non-aromatics (chloroform, dichloromethane). This is likely because the aromatic solvents are "better" solvents for aromatic MEH-PPV, like dissolves like. The better solvents promote extension of the polymer chain. This results in longer conjugation lengths (chromophores) and increased intra-chain transfer. Work by Zheng, Fenglian, and Zhu confirms the slight red shift of the absorption spectra in aromatic solvents compared with that of aliphatic solvents [Zheng, 1998]. Work by Zahid, Saad, and Mahmood found the aromatic solvent xylene gave optimum performance for both electrical and optical properties compared to the poor performance of the non-aromatic solvent chloroform when they were used with MEH-PPV to form a Titanium Dioxide active layer in a solar cell [Zahid, 2012]. This illustrates the importance of the additional red shift obtained by the aromatic solvents.

Third, the stability of a molecule can be determined by its potential energy found in Gaussian. The lower energy molecule is more stable. The energy found in Gaussian using for our decamer model in all five solvents was -8126.1 au. The energy found in Gaussian for our stacked pentamer model in all five solvents was -8127.3 au. The stacked model is more stable and therefore more likely to occur.

Figure 6.6 compares the single pentamer with the single decamer model data. Although the decamer is twice as long as the single pentamer, the lack of red-shift in chlorobenzene indicates that the chain is not coiling back on itself. The chain is not demonstrating strong inter-chain transfer (inter-chain aggregation) between two parts of the same chain. Work by Ben Schwartz confirms the fact that the decamer is not folding onto itself and therefore there is no resulting inter-chain transfer. Conjugated polymers are stiff enough that it is difficult to fold a chain to bring two straight conjugated segments into the parallel configuration necessary for inter-chain delocalization [Schwartz, 2003].

6.7 Dipole Moment

It is of interest that in the experimental data and the stacked model, chlorobenzene shows by far the largest red shift, but in the decamer model, both toluene and xylene show bigger red shifts. The reason for this could be related to the dipole moment. Chlorobenzene has a dipole moment of 1.54, whereas toluene's dipole moment is 0.31 and xylene's is 0.45. The calculated dipole moments of the molecules in the ground and excited state are given in Table 6.2.

Table 6.2: Dipole moment of solvents and pentamers in each solvent. Dipole Moment for molecule in ground and excited states calculated by Gaussian

	Dipole Moment of Solvent (Debye)	Dipole Moment of molecule ground state (Debye)	Dipole Moment of molecule excited state (Debye)
Gas		3.76	4.07
Toluene	0.31	4.30	4.71
Xylene	0.45	4.30	4.71
Dichloromethane	1.14	4.73	5.20
Chloroform	1.15	4.58	5.06
Chlorobenzene	1.54	4.63	5.11

In addition to the ground state, the first excited state of the pentamer in all solvents was optimized in Gaussian in order to find the dipole moment in the excited state. If the excited-state dipole moment is smaller than that of the ground state then increasing the polarity of the environment will stabilize the ground state more than the excited state. Conversely, if the excited-state dipole moment is larger than that of the ground state then increasing the solvent polarity will stabilize the excited state more than the ground state [Schwartz, 2003]. In all solvents the excited state dipole moment is higher than the ground state dipole moment. Therefore, the higher polarity of chlorobenzene stabilizes the excited state more in chlorobenzene than in toluene and xylene. This means that the inter-chain interactions in the stacked pentamer chlorobenzene model are more stabilized and produce a larger red shift than the stacked pentamers in toluene and xylene. In contrast, the decamer in chlorobenzene is a well isolated chain and only has intra-chain interaction. The polarity stabilizing the excited state does not red shift the decamer as much as the inter-chain interaction of the stacked pentamers.

This work with interchain and intrachain interactions illustrated the fact that the trends between the theoretical and experimental UV-Vis absorption values were comparable, however, the absolute magnitudes of the absorption peaks from experimental data were consistently lower (blue-shifted) relative to those from the theoretical data. It was desired to find a way of modelling the oligomers to theoretically match the absolute values of the experimental data that lead us to the work described in chapter 7. Up until this point the functional being used was the popular global hybrid functional B3LYP and the basis set was 6-31G. In Chapter 7 a new combination of functional and basis set are used to find a more accurate way to model MEH-PPV.

Chapter 7

Advanced Modelling with Range Separated Functionals

In work up to this point, the absolute magnitudes of the absorption peaks from experimental data were consistently lower relative to those from the theoretical data. In order to improve the correlation between experimental and computational measurements of the absorption behavior of MEH-PPV, the following work was conducted and is reported here:

- UV-VIS measurements were taken using different solvents and known MEH-PPV polymer chain lengths. [Tilley 2011]
- RS functionals wB97XD and CAM-B3LYP incorporated in Gaussian were used to better model MEH-PPV ground and excited states.
- Successively more accurate basis sets were tested in order to determine the best basis set able to yield results in agreement with experiment.
- The UV-VIS experimental data was used to calibrate ω.
- Different cases were modeled using the newly found ω values.

7.1 Range Separated Functionals

As discussed in Chapter 4, hybrid functionals such as B3LYP are unable to correctly predict electronic transitions of conjugated systems involving the charge transfer process [Bhatta, 2015] [Korzdorfer, 2011; Avhad, 2017; Borpuzari, 2017; Yanai, 2004; Refaely-Abramson, 2011; Chai, 2008; Sekar, 2018; Pandey, 2012]. Range-separated (RS)

functionals have been created to overcome this problem. In RS-functionals, the range separation parameter ω is employed in order to switch between the Density Functional Theory and Hartree-Fock methods for modeling the system. wB97XD and CAM-B3LYP are examples of RS functionals. The default values of ω for the RS-functionals are set to a specific number. However, the default values consistently give UV-Vis peak values lower than experimental values [Bhatta, 2015].

This study used the two RS functionals, CAM-B3LYP and wB97XD. The computed result's accuracy from both these functionals, however, depends on the range-separation parameter ω. Previous research (Tables 7.1 and 7.2) [Bhatta, 2015; Korzdorfer, 2011; Refaely-bramson, 2011; Pandey, 2012; Lima, 2014; Nenon, 2014; Kastinen, 2016; Kityk, 2014] indicates that the values for ω that produce accurate orbital energies in conjugated systems are much lower that the default values for CAM-B3LYP (ω=0.33) and wB97XD (ω=0.2). Tables 7.1 and 7.2 give a listing of ω values found for polymers and molecules in previous studies. One goal of the work reported here was to determine the most accurate range separation parameter values for modeling MEH-PPV of various chain lengths as well as investigating the effect of different solvents.

Table 7.1: Range-Separation parameter (ω) optimized for various polymers

Polymer	**Omega (bohr^{-1})**	**Functional/Basis Set**	**# repeat units where saturates**	**reference**
PCzBT	0.164	LC-BLYP/6-31G(d,p)	3-4	[Lima, 2014]
PCzTP	0.138	LC-BLYP/6-31G(d,p)	3-4	[Lima, 2014]
PCzTH-TVDCN	0.156	LC-BLYP/6-31G(d,p)	3-4	[Lima, 2014]]
PTTh-TVDCN	0.162	LC-BLYP/6-31G(d,p)	3-4	[Lima, 2014]
PCDTBT	0.152	wB97/6-31G(d,p)	2-3	[Pandey, 2012]
PBDTTPD	0.125	wB97/6-31G(d,p)	4	[Pandey, 2012]
PBDTTT-C	0.117	wB97/6-31G(d,p)	4	[Pandey, 2012]
PBDTTT-CF	0.117	wB97/6-31G(d,p)	4	[Pandey, 2012]
PBDTTT-E	0.117	wB97/6-31G(d,p)	4	[Pandey, 2012]
PCPDTBT	≈0.1	wB97/6-31G(d,p)	Over 6	[Pandey, 2012]
PBT	0.145	CAM-B3LYP/6-31G(d)	6	[Nenon, 2014]
PDA	0.166	CAM-B3LYP/6-31G(d)	6	[Nenon, 2014]
O3p	0.10	wB97XD/6-31G(d)	Copolymer/trimer	[Kastinen, 2016]
$C_{2n}H_{4n+2}$	0.267	LC-BNL/cc-pVTZ	7	[Korzdorfer, 2011]

Table 7.2: Range-Separation parameter (ω) optimized for various small molecules

Molecule	**Omega (bohr^{-1})**	**Functional/Basis Set**		**reference**
$PC_{61}BM$	0.15	wB97XD/6-31G(d)	Fullerene derivative	[Kastinen, 2016]
$PC_{71}BM$	0.13	wB97XD/6-31G(d)	Fullerene derivative	[Kastinen, 2016]
oligothiophenes	0.148	wB97/6-31G(d,p)		[Pandey, 2012]
Thiophene	0.313	BNL/cc-pVTZ		[Refaely-Abramson, 2011]
Thiadiazole	0.355	BNL/cc-pVTZ		[Refaely-Abramson, 2011]
Benzothiazole	0.288	BNL/cc-pVTZ		[Refaely-Abramson, 2011]
Benzothiazole	0.293	BNL/cc-pVTZ		[Refaely-Abramson, 2011]
Fluorine	0.240	BNL/cc-pVTZ		[Refaely-Abramson, 2011]
PTCDA	0.207	BNL/cc-pVTZ		[Refaely-Abramson, 2011]
C_{60}	0.211	BNL/cc-pVTZ		[Refaely-Abramson, 2011]
H_2P	0.252	BNL/cc-pVTZ		[Refaely-Abramson, 2011]
4-(9-acridyl)julolidine	0.245	LC-BLYP/6-31+G(d,p)		[Kityk, 2014]
M1-M12	0.10-0.15	LC-BLYP/6-31G(d)	Small conjugated molecules (SCM)	[Bhatta, 2015]

7.2 Choice of Basis set

In order to perform calculations in Gaussian, it is necessary to select a basis set. In previous work [Giri, 2014], the basis set, 6-31G was chosen. However, the model accuracy can be improved by selecting increasingly complex basis sets.

Testing was done on an MEH-PPV dimer in order to see the effects of changing the basis set on UV-Vis peak absorption. The results of using a sequence of successively more accurate basis sets using the RS functionals wB97XD and CAM-B3LYP with the default values of ω are seen in Figure 7.1.

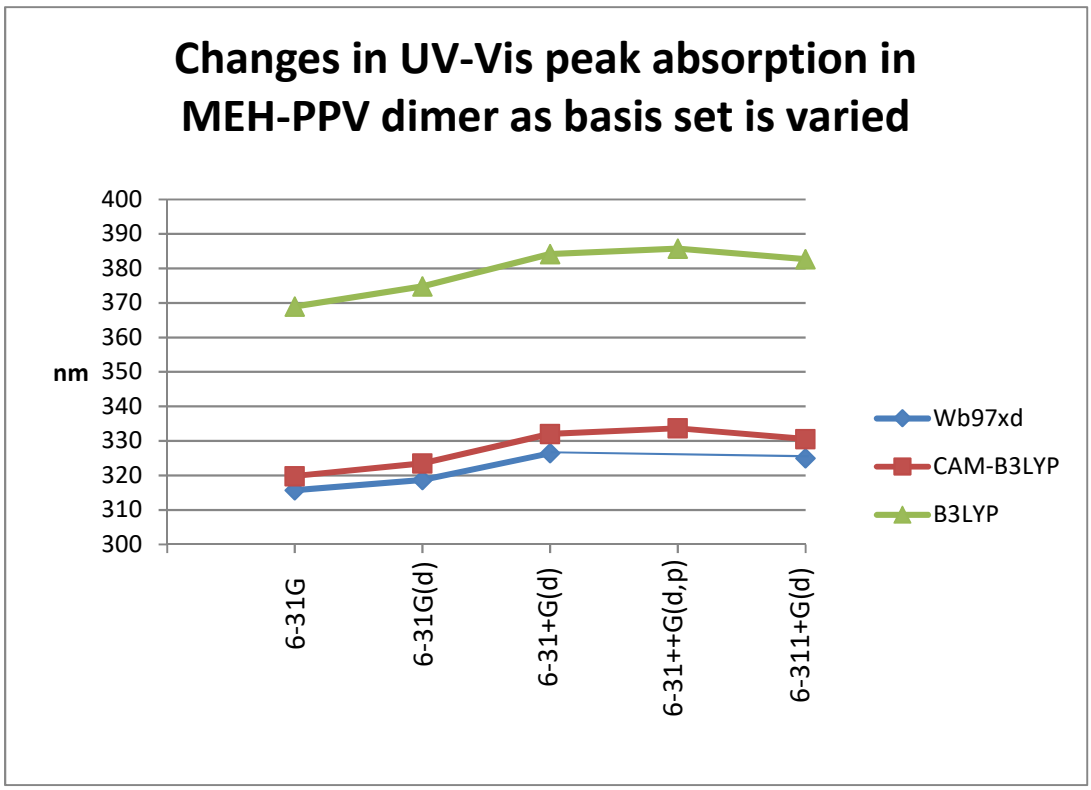

Figure 7.1: Comparison of Basis Sets

In Figure 7.1, the RS functionals with varying basis sets are compared to the wavelength associated with peak absorption for a dimer using the GS functional B3LYP and the basis set 6-31G (371.46 nm). It is clear that the RS functionals closely agree with one another and the B3LYP value is more than 50 nm higher than the RS values with the same basis set. For an MEH-PPV dimer, Gaussian converges using either RS functional and each of the increasingly complex basis sets (excluding one). However, as the polymer chain length increases, the calculations become more difficult and computational limitations become a major factor. Attempts were made at modeling a trimer using the 6-31G+(d) basis set. For the trimer, the RS functional wb97xd combined with basis set 6-31G+(d) resulted in non-convergence. Even the results using non-RS functional B3LYP combined with the 6-31G+(d) basis set did not converge. Therefore, given current computing limitations, it was not possible to obtain convergence for the MEH-PPV trimer or longer oligomers using the 6-31+G(d) basis set. The most complex basis set that achieved convergence for polymer chains longer than a dimer was 6-31G(d). Nonetheless, 6-31G(d) is a good basis set for optimizing the ground state geometry and has been the choice for many other research groups doing similar work [Bhatta, 2015; Nenon, 2014; Kastinen, 2016; Hirao, 2011].

Although it was not possible to achieve convergence with the more complex basis sets, this challenge can be overcome in part by selection of the appropriate range-separation parameter ω as described below.

7.3 Optimization of the Range-Separation Parameter ω

Both CAM-B3LYP and wB97XD have a default value for the range separation parameter. The default value for CAM-B3LYP is 0.33 and the default value for wB97XD is

0.20. It has been observed that accurate orbital energies for conjugated systems are predicted using much smaller values for ω than the default values [Bhatta, 2015]. The main effect of the ω parameter is to control the length scale for range separation. In other words, ω controls the screening of the Coulomb interaction in the system [Korzdorfer, 2011].

In order to optimize the range separation parameter, computational data for UV-Vis peak absorption was compared to experimental data. Different ω values were tested until the theoretical UV-Vis results best matched the experimental data. Experimental data for trimer, tetramer, and pentamer of MEH-PPV in five different solvents was available. These solvents are Chloroform, Chlorobenzene, Dichloromethane, Xylene, and Tetrahydrofuran. Using a simple grid search optimization and comparing the computational data to the experimental data, the closest match to three decimal places for the range separation parameter for trimer, tetramer, and pentamer in these 5 solvents was found. Optimizing of the ω values was performed using two different RS functionals, wB97XD and CAM-B3LYP, for both ground state geometry optimization and TD-DFT. The 6-31G(d) basis set was used in conjunction with both functionals. PCM was used to theoretically model the different solvents. The ω values tuned to 3 decimal places for trimer, tetramer and pentamer in five different solvents are seen in Table 7.3.

Table 7.3: Range separation parameter values optimized to three decimal places for MEH-PPV trimer, tetramer, and pentamer in 5 solvents

Oligomer	**Solvent**	**Experiment**	**wB97XD**	**wB97XD**	**CAM-B3LYP**	**CAM-B3LYP**
		nm	**ω bohr^{-1}**	**Absorption nm**	**ω bohr^{-1}**	**Absorption nm**
Trimer	Chlorobenzene	400.0345	0.125	400.17	0.215	400.04
	Xylene	396.94	0.125	396.85	0.220	396.8
	DCM	396.94	0.130	396.82	0.220	397.57
	Chloroform	396.94	0.128	397.19	0.220	397.12
	THF	396.94	0.129	396.74	0.220	397.03
Tetramer	Chlorobenzene	435.036	0.101	434.55	0.190	435.42
	Xylene	433.037	0.101	433.37	0.191	433.21
	DCM	433.037	0.103	432.1	0.193	433.15
	Chloroform	431.96	0.103	431.7	0.195	432.03
	THF	429.96	0.106	429.67	0.200	430.09
Pentamer	Chlorobenzene	458.057	0.101	458.33	0.192	458.18
	Xylene	454.9945	0.102	455.27	0.194	455.35
	DCM	454.075	0.106	454.22	0.198	454.58
	Chloroform	454.075	0.105	454.2	0.198	454.15
	THF	451.93	0.108	452.12	0.200	453.24

7.4 Comparison to default ω values

The previous study reported computational and experimental results for trimer, tetramer, and pentamer in chloroform [Giri, 2014]. These calculations were done using the GH functional B3LYP and the 6-31G basis set. In the present study, the work has been repeated using the long-range corrected RS functionals CAM-B3LYP and wB97XD and the basis set 6-31G(d). Table 7.4 shows the experimental data, the previous computational results, and the new data using the default omega for both functionals as well as the omega values optimized to 3 decimal places for three lengths of MEH-PPV in chloroform. The results for wavelength corresponding to the UV-Vis peak absorption that were calculated using these optimized ω values align well with experimental results.

Table 7.4: UV-Vis wavelength (nm) for different length monomers of MEH-PPV in chloroform solution

MEH-PPV Oligomer	**Experiment [19] experiment-al results**	**Theory Functional: B3LYP Basis set: 6-31G No Omega: B3lyp not RS**	**Theory Functional: wB97XD Basis Set: 6-31G(d) Default Omega=0.2**	**Theory Functional: wB97XD Basis Set: 6-31G(d)**	**Theory Functional: CAM-B3LYP Basis Set: 6-31G(d) Default Omega= 0.33**	**Theory Functional: CAM-B3LYP Basis Set: 6-31G(d)**
3	397 nm	435 nm	367 nm	397 nm Omega= .128	375 nm	397 nm Omega= .22
4	432 nm	482 nm	379 nm	432 nm Omega= .103	397 nm	432 nm Omega= .195
5	454 nm	518 nm	395 nm	454 nm Omega= .105	415 nm	454 nm Omega= .198

Previous studies have acknowledged that RS functionals with default values for ω consistently give higher lying LUMO energies, lower lying HOMO energies, bigger HOMO-LUMO gaps, and higher vertical excitation energies for conjugated systems when compared to experimental values [Bhatta, 2015; McCormick, 2013]. Tuning the value of ω affects the HOMO and LUMO energies. A smaller ω value decreases the HOMO-LUMO gap. RS functionals like wB97XD and CAM-B3LYP with their default ω values overestimate the HOMO/LUMO and optical gaps compared to experimental values. This

overestimation of the optical gap is demonstrated using default values for ω as compared to optimized ω values and experimental values in Table 7.4.

7.5 Range-Separation parameter ω vs number of monomer units

In the previous study [Giri, 2014] peak UV-Vis absorption was found theoretically for MEH-PPV chains 1-10 monomers in length. In that study, it was found that the peak absorption wavelength changed very little beyond a pentamer and that a pentamer was a good model for MEH-PPV in solution. Similarly, in the present study, it appears that the value of the range-separation parameter ω stabilizes as the chain length reaches 4 to 5 monomers (see Table 7.3). This agrees with the literature. Korzdorfer et al concluded that the optimal ω value depends on the π-conjugation of the system and optimized ω values decrease with increasing chain length. They suggested that employing a single range-separation parameter is likely to yield a reasonable approximation for saturated molecules [Korzdorfer, 2011].

Therefore, the ω value we used for RS functional computational model on longer polymer chains was the ω value found for a pentamer, rounded to 2 decimal places. The ω values used for wB97XD and CAM-B3LYP were 0.11 and 0.20, respectively. These ω values are refereed to as "tuned" ω values for CAM-B3LYP and wB97XD as the effects solvent, effects of chain length, and comparison with default ω values for both functionals are studied.

Table 7.5 compares the experimental and computational values using both the default ω values and the tuned ω values. A significant difference is observed in wavelength

values corresponding to UV-Vis peak absorption between experimental values and theoretical values obtained using default values for ω. Previous studies have found tuned values for ω to fall between 0.1 and 0.20 $Bohr^{-1}$ when working with small conjugated molecules (SCMs) and polymers [Bhatta, 2015; Pandey, 2012; Lima, 2014; Nenon, 2014; Kastinen, 2016].

Table 7.5: Comparison of computational results using default and tuned ω values

Oligomer	**Solvent**	**Experiment nm**	**wB97XD nm**	**wB97XD nm**	**CAM-B3LYP nm**	**CAM-B3LYP nm**
			Default ω=0.20 $bohr^{-1}$	Tuned ω=0.11 $bohr^{-1}$	Default ω=0.33 $bohr^{-1}$	Tuned ω=0.20 $bohr^{-1}$
Trimer	Chlorobenzene	400.0345	368.08	405.62	376.14	404.34
	Xylene	396.94	365.7	403.9	374.35	402.45
	DCM	396.94	367.63	404.37	375.2	403.17
	Chloroform	396.94	366.6	404.09	374.78	402.74
	THF	396.94	367.03	403.86	374.71	402.61
Tetramer	Chlorobenzene	435.036	380.74	428.69	398.24	431.76
	Xylene	433.037	378.48	427.08	396.43	429.92
	DCM	433.037	380.29	427.61	397.45	430.63
	Chloroform	431.96	379.49	427.18	396.95	430.23
	THF	429.96	379.78	427.07	396.96	430.09
Pentamer	Chlorobenzene	458.057	396.05	451.91	416.37	454.79
	Xylene	454.9945	392.67	449.27	414.34	452.82
	DCM	454.075	396	451.11	415.64	453.75
	Chloroform	454.075	394.68	450.28	415.22	453.34
	THF	451.93	395.36	450.53	415.2	453.24

It is clear that the tuned value of ω yields results much more in agreement with the experimental results than the results using default ω values. This is true even though the same ω value was used for all the solvents.

7.6 Effect of Chain Length

Using range separated functionals with the tuned ω values (0.11 for wB97XD and 0.20 for CAM-B3LYP) and the 6-31G(d) basis set allows the model to yield values that match the experimental results. Figure 7.2 shows the difference between the experimental values and the theoretical values for trimer, tetramer, and pentamer. The theoretical values we obtained for the non-range separated functional B3LYP are included with values using RS functionals wB97XD and CAM-B3LYP with default and tuned range separation parameter values.

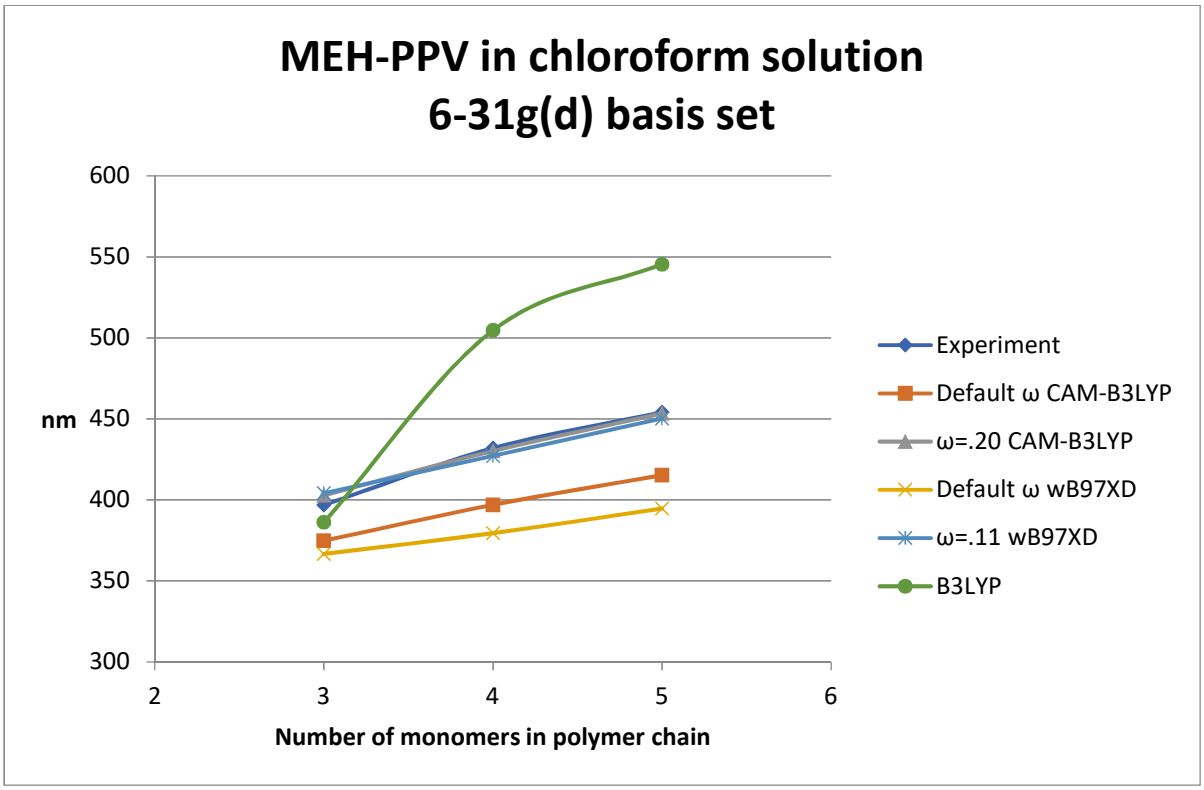

Figure 7.2: Experimental and Theoretical UV-Vis peak absorption in trimer, tetramer, and pentamer

Thanks to the optimization of the range-separation parameter, the values obtained with CAM-B3LYP and wB97XD with tuned ω values are very close to the experimental values (see Table 7.4). The RS functionals with the default values of ω are considerably lower than the experimental values. The values for B3LYP deviate with the experimental values even more greatly as they are much higher.

Experimental results for polymer chains longer than a pentamer were not available. As can be seen from the graphs, when the ω value is "tuned", there is great correlation between experimental and theoretical data. This is especially true once the chain length reaches 4 monomer units; the ω value then saturates and does not change significantly as the

chain grows longer. This saturation of the characteristic length scale of the range separation (1/ω) has been seen in several studies and is indicated in Table 7.3. As explained in the previous section, using the tuned values of ω from the pentamer experiments has been shown to give a good prediction of the absorption peak [Giri, 2014; Korzdorfer, 2011]. Figure 7.3 shows the theoretical UV-Vis peak absorption data for MEH-PPV chains in chloroform from 3 to 10 monomers. Included is previous data [Giri, 2014] using the B3LYP functional and 6-31G basis set as well the new theoretical data using RS functionals CAM-B3LYP and wB97XD with tuned ω values and the 6-31G(d) basis set.

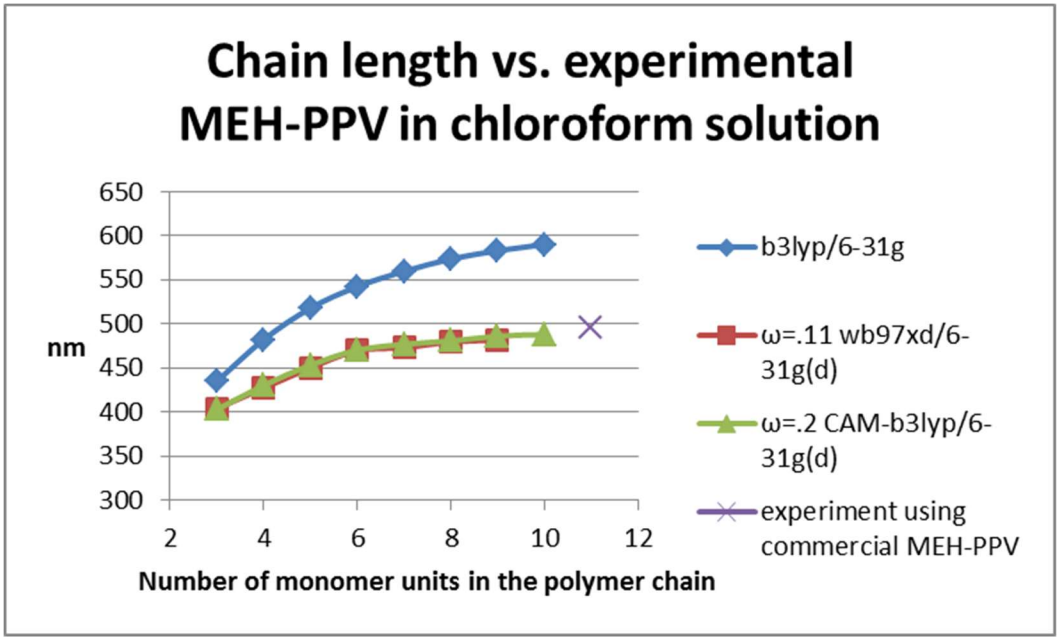

Figure 7.3: Experimental and Theoretical UV-Vis peak absorption for MEH-PPV chain length 3 to 10 monomer units

Although work has been done experimentally and computationally with specific lengths of polymer chains, one must remember that absorption is actually controlled by the conjugation length of the chromophores and not the chain length. Increasing the chain length does not necessarily affect the conjugation length of the chromophores within the conjugated backbone, but the conjugation length cannot exceed the chain length [Traiphol, 2010]. Conjugation lengths ranging from two to twelve monomer units have been reported for MEH-PPV [Yamagata, 2014; Collini, 2009]. In previous work [Giri, 2014] a five monomer unit was chosen for our theoretical model of an MEH-PPV polymer chain. Kohler, Hoffman and Bassler agreed with this choice as they reported that at room temperature MEH-PPV chains have effective conjugation lengths of about five repeat units [Kohler, 2012].

Figure 7.3 compares the computed values for lengthening MEH-PPV chains in chloroform to the experimental value for dilute solution of commercial MEH-PPV in chloroform (496 nm). The experimental value of 496 nm is slightly higher than the RS theoretical values for the MEH-PPV decamer. In solution the exact conjugation lengths of the chromophores is not known. Also in solution there could be multiple polymer chains interacting with each other as π-electrons on one chain overlap with the neighboring chain. This is known as π-π stacking in inter-chain aggregation [Kohler, 2012; Schwartz, 2003]. This aggregation causes a red shift in the absorption spectrum. From this the conclusion can be reached that the chromophore length of MEH-PPV in solution is probably longer than our initial choice of the pentamer and that there is inter-chain aggregation causing a red shift. The fact that a small red shift between experimental and computational results can be attributed to intermolecular interactions that occur in inter-chain aggregation in

experimental measurements but are not present in computed results was also the conclusion of the study by Bhatta's group [Bhatta, 2015].

7.7 Effect of Solvent

There are several variables to consider when studying absorption in MEH-PPV in solution. One variable is the solvent. Figure 7.4 and 7.5 compare the experimental results obtained for MEH-PPV trimer, tetramer, and pentamer in 5 solvents to the computational results we calculated for the same length polymers in the same 5 solvents. The five solvents were chlorobenzene, DCM, Chloroform, THF, and xylene. The theoretical results displayed in Figure 7.4 were obtained using the RS functional wB97XD and the basis set 6-31G(d) along with the tuned range-separation parameter ω=0.11. The theoretical results displayed in Figure 7.5 were obtained using the RS functional CAM-B3LYP and the basis set 6-31G(d) along with the tuned range separation parameter ω=0.20.

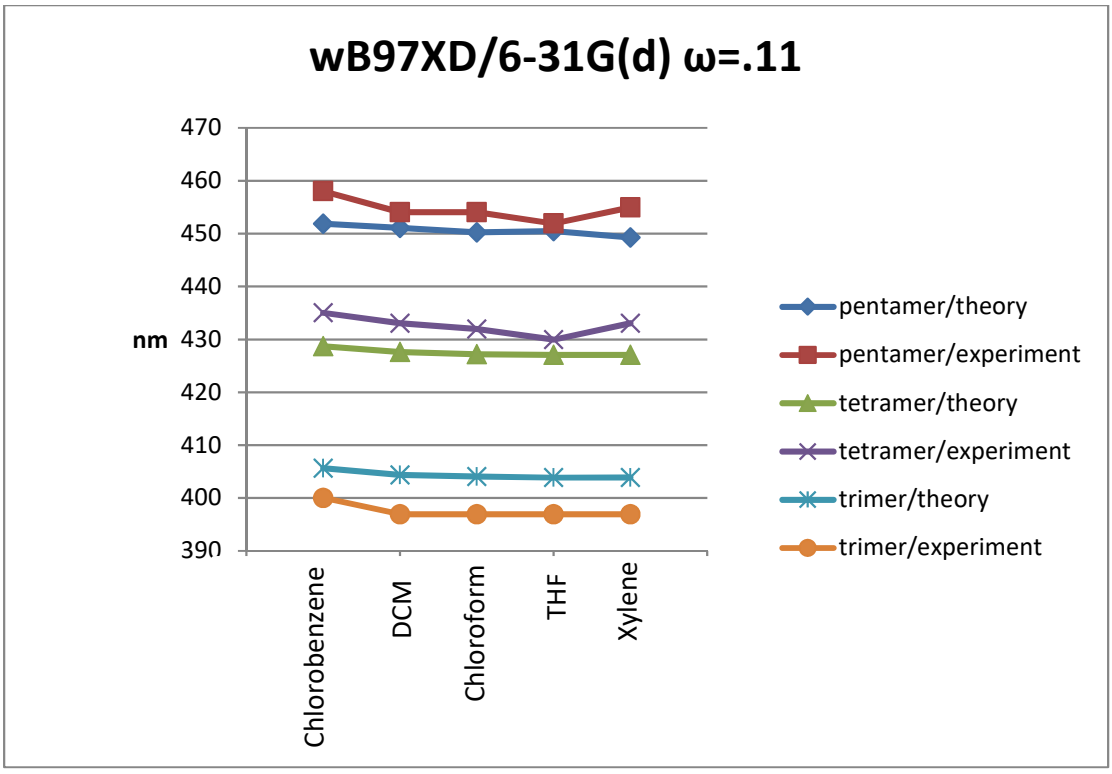

Figure 7.4: Experimental and computational results using wB97XD functional and tuned ω= 0.11 $bohr^{-1}$ for UV-Vis peak absorption in Meh-PPV pentamer, tetramer, and trimer in 5 solvents

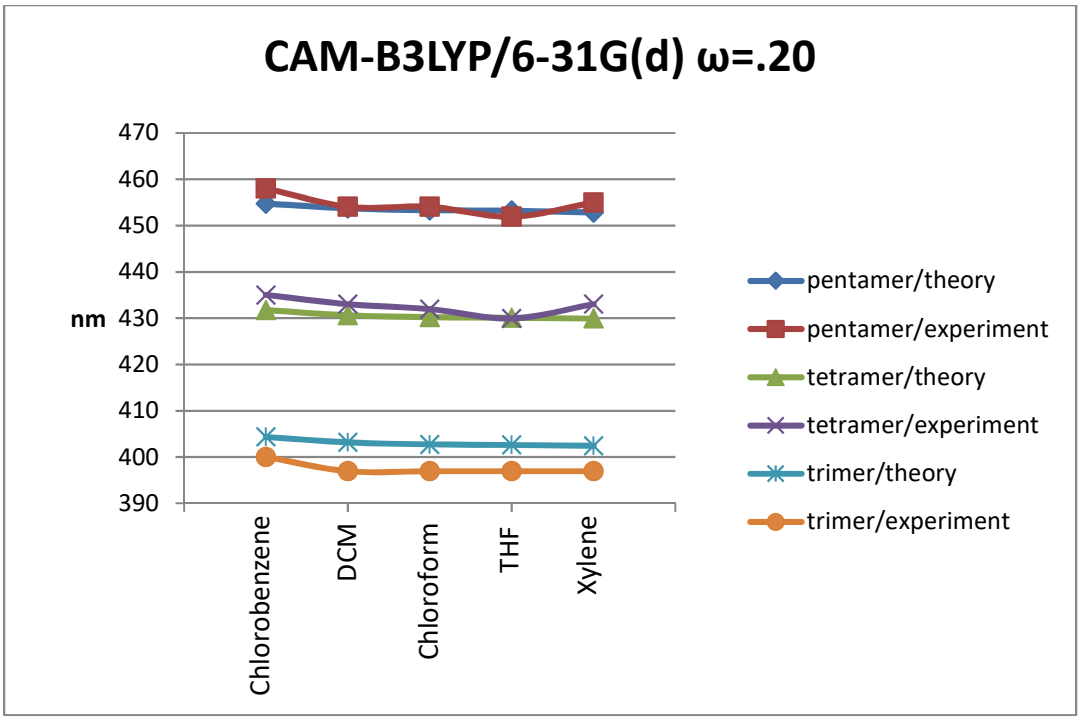

Figure 7.5: Experimental and computational results using CAM-B3LYP functional and tuned ω=0.20 $bohr^{-1}$ for UV-Vis peak absorption in MEH-PPV pentamer, tetramer, and trimer in 5 solvents

As seen in Figures 7.4 and 7.5, the differences in the UV-Vis peak absorption between different solvents is small. However, as can be seen from the data in Table 7.4, the differences between the solvents are not non-existent.

To investigate the accuracy of the theoretical results, the accuracy of +/-0.07nm that was found in the experimental results was utilized. Using the value for UV-Vis peak absorption for a pentamer in chloroform of 454.075 +/-0.07 nm, the most accurate values for ω were found to 4 decimal places. It was found that an experimental error of 0.07nm corresponds to Δω=0.0002 for CAM-B3LYP and Δω=0.0001 for wB97XD. If ω values for two different solvents differ by more than 0.0004 (= 2* Δω) for CAM-B3LYP or 0.0002 (2*

Δω) for wB97XD, then the ω values are significantly different. As seen in Figures 7.6 and 7.7, this is, in fact, the case. Using an ω with a precision of 4 digits allows us to distinguish between the solvents. Figures 7.6 and 7.7 illustrate this with error bars for the ω in different solvents.

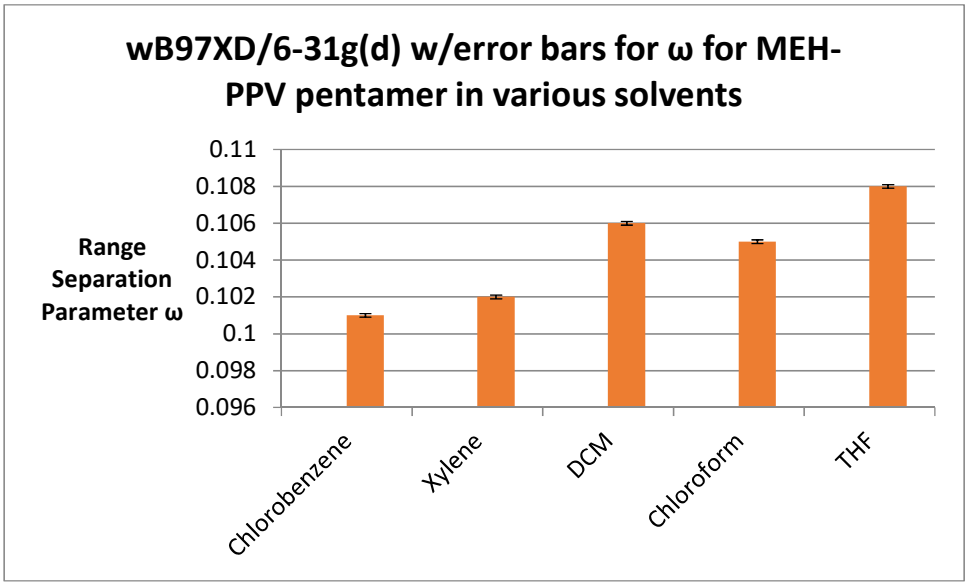

Figure 7.6: Range separation parameter with error bars for MEH-PPV pentamer in five solvents using wB97XD functional

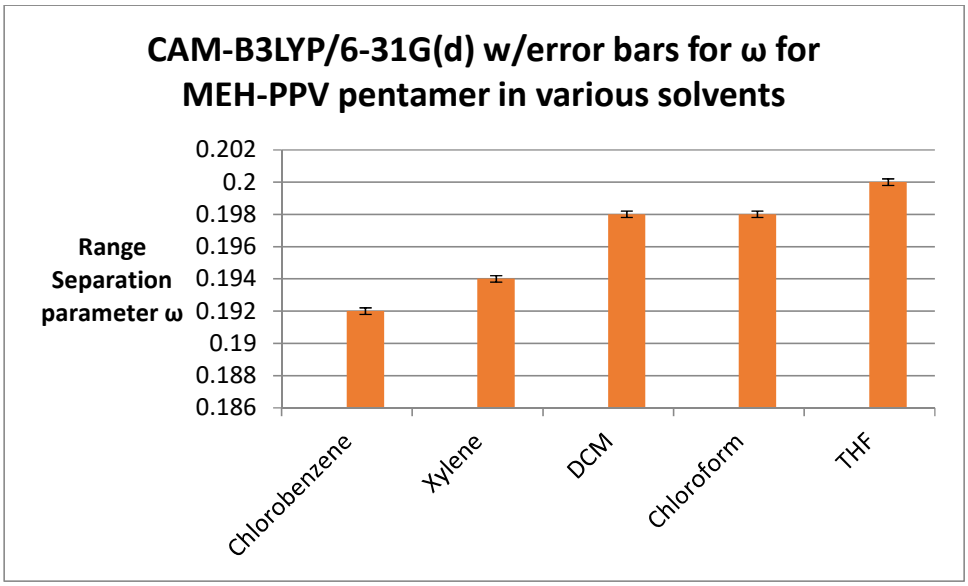

Figure 7.7: Range separation parameter with error bars for the MEH-PPV pentamer in five solvents using CAM-B3LYP functional

Though small, the differences indicate that the solvent does have an effect on Coulomb screening [Korzdorfer, 2011]. Chlorobenzene was consistently the most red-shifted and had the lowest ω value. This was true of both wB97XD and CAM-B3LYP functionals. The highest value for ω was consistently for THF. THF was always the least red-shifted. Generally speaking, among the different solvents, a greater red shift brings a lower ω value.

The conformation of polymer chains in solution depends on both the solvent used and the polymer concentration [Nguyen, 1999; Traiphol, 2010; Schwartz, 2003; Quan, 2006]. Chlorobenzene is known as a "good solvent" where polymer backbone-solvent interactions are favorable and the polymer chain adopts an open, extended conformation. THF is known as a "poor solvent" where polymer backbone-solvent interactions are not favorable and the polymer twists and coils to avoid these interactions. This twisting and

coiling can break the conjugation length of the polymer chain, causing shorter conjugation lengths [Nguyen, 1999; Traiphol, 2010; Schwartz, 2003].

The conjugation lengths of the polymer chains have a great influence on absorption. [Traiphol, 2010; Lampert, 2014]. Longer conjugation lengths cause the absorption spectrum to red shift [Nguyen, 1999; Traiphol, 2010; Collison, 2001; Zhu, 2009]. The torsion angle of the conjugated backbone determines the conjugation length [Quan, 2006]. Collapsed chains resulting from a poor solvent can break the conjugation lengths and therefore a blue shift from the previously longer conjugation lengths. Although there are only very small differences in the wavelength values for different solvents, it appears that a "better" solvent has a slightly smaller ω value and the characteristic length scale over which the treatment of the Coulomb operator changes from SR to LR increases slightly with the decreasing ω [Korzdorfer, 2011]. The effect of a twisted structure on the range separation parameter was seen in a study by Lima et al. Tetramers of planar PCzTP were found to have a smaller ω value than the more twisted PCzBT structure.

Chapter 8

Conclusion

The study began with first principles calculations based on density functional theory with hybrid functional B3LYP for exchange-correlation potential. These calculations were carried out to understand the origin of the red shift in the photo absorption peak in electrospun MEH-PPV polymer. The effects of polymer chain length, stretching of the C=C double bond linking the monomer units, and the solvent on the shift in the photo absorption peak were studied separately. All three of these parameters were seen to cause a red shift, but further understanding the polymer chains in solution was desired.

In order to study the effects of polymer morphology on the absorption spectrum, models of MEH-PPV in pentamer, decamer and stacked pentamer forms were created. All were created using the functional B3LYP and the basis set 6-31G. Interchain and intrachain interactions in different solvents were studied using these models. Overall, these results indicate that inter-chain interactions play a critical role in real solutions. The fact that the stacked pentamer model more closely corresponds to the experimental results would indicate that the red-shifting seen experimentally is affected by inter-chain aggregation that results from overlapping polymer chains. In the debate over the fraction of photoexcitations that result from inter-chain species, our results would support that inter-chain species are a critical factor. Furthermore, our results indicate that in aromatic solvents inter-chain aggregation takes precedence over intra-chain interaction.

Finally, in order to find models that more accurately correlate with experimental results, range-separated functionals were used. Optimized range separation parameters were found for two RS functionals for MEH-PPV of three different lengths in five different solvents using experimental data. The differences in the optimized range separation parameter (ω) values were significant when varying the solvent. In addition, the optimized ω value for tetramer and pentamer were very similar implying that the ω value for a pentamer could be used for longer MEH-PPV chains. With these conclusions, a tuned ω value was determined for the RS functionals CAM-B3LYP and wB97XD when testing MEH-PPV. A range from 0.1 to 0.2 $bohr^{-1}$ was found to be appropriate for the polymer MEH-PPV.

Using these tuned range separation parameters, UV-Vis results were compared to results using the default ω values for both functionals. Previous studies with different molecules have found that RS functionals with default values for ω overestimate HOMO/LUMO and optical gaps when compared to experimental values. This was confirmed to be true with the polymer MEH-PPV. The tuned ω values found were obviously much more accurate in predicting experimental values. Comparing the UV-Vis data to previous results using the GS hybrid functional B3LYP and data using RS-functionals with tuned ω, it was illustrated how vastly improved the results are for RS functionals when modeling the excited state.

Early in the study it was determined that the conjugation length for MEH-PPV that most accurately modeled the polymer was a pentamer. Now comparing the experimental data from commercial MEH-PPV in dilute chloroform solution and the much more accurate theoretical data for MEH-PPV of lengths from three to ten monomers, it is speculated that

the conjugation length is actually much longer. A longer conjugation length would cause a red shift. Also, it is predicted that aggregation between MEH-PPV chains is occurring in solution and this also causes a red shift.

Although there are small differences in the wavelength values for different solvents, these differences are statistically significant. It was found that "better" solvents (like chlorobenzene) have slightly smaller range-separation parameters (ω). This means that the characteristic length scale over which the treatment of the Coulomb operator changes from short range to long range is larger for good solvents. Generally speaking, among the different solvents, good solvents bring a greater red shift and a lower ω value than poor solvents. This may offer opportunities for better understanding of polymer/solvent interaction.

The data found using the tuned ω values for CAM-B3LYP and wB97XD are close to one another. Since CAM-B3LYP is much faster computationally than wB97XD and the results are comparable, it may be beneficial to use CAM-B3LYP instead of wB97XD for this type of problem.

References

1. Avhad, K.; Jadhav, A.; Sekar, N. Flourescent vinyl and styryl coumarins: A comprehensive DFT study of structural, electronic and NLO properties. *Journal of Chemical Science* **2017**, *129,* 1829-1841.
2. Bauernschmitt, R.; Ahlrichs, R. Treatment of electronic excitations within the adiabatic approximation of time dependent density functional theory. *Chem. Phys. Lett*. **1996**, *256,* 454-64.
3. Bhatta, R. S.; Pellicane, G.; Tsige, M. Tuning range-separated DFT functionals for accurate orbital energy modeling of conjugated molecules. *Computational and Theoretical Chemistry* **2015,** *1070,* 14-20.
4. Blom, P.; Mihailetchi, V.; Koster, A.; Matkov, D. Device Physics of Polymer: Fullerene Bulk Heterojunction Solar Cells. *Advanced Materials* **2007**, *19,* 1551-1566.
5. Borpuzari, M. P.; Kar, R. A New Nonempirical Tuning Scheme with Single Self-Consistent Field Calculation: Comparison with Global and IP-Tuned Range-Separated Functional. *Journal of Computational Chemistry* **2017**, *38,* 2258-2267.
6. Chai, J.; Head-Gordon, M. Long-range corrected hybrid density functionals with damped atom-atom dispersion corrections. *Physical Chemistry Chemical Physics* **2008**, *10*, 6615-6620.
7. Chang, R.; Hsu, J. H.; Fann, W. S.; Liang, K. K.; Chang, C. H.; Hayashi, M.; Yu, J.;Lin, S. H.; Chang, E.C.; Chuang, K.R.; Chen, S.A. Experimental and theoretical investigations of absorption and emission spectra of light-emitting polymer MEH-PPV in solution. *Chemical Physics Letters* **2000**, *317*, 142-152.
8. Chiu, M.; Kee, T. W.; Huang, D. M. Coarse-Grained Simulations of the Effects of Chain Length, Solvent Quality, and Chemical Defects on the Solution-Phase Morphology of MEH-PPV Conjugated Polymers. *Australian Journal of Chemistry* **2012**, *65*, 463-471.
9. Clark, J., "The Beer-Lambert Law," www.chemguide.co.uk, (2007).
10. Collini, E.; Scholes, G. D. Coherent Intrachain Energy Migration in Conjugates Polymer at Room Temperature. *Science* **2009**, *323*, 369-373.

11. Collison, C. J., Rothberg, L. J., Treemaneekarn, V. and Li, Y. Conformational Effects on the Dynamics. *Macromolecules* **2001**, *34,* 2346-2352.
12. Fazlinashatul, S. Z.; Puteri, S. M. S.; Mahmood, M. R. Solvent Effects on the Electrical and optical Properties of Nanocomposited MEH-PPV: TiO Films for Organic Solar Cells Application. *Advance Materials Research* **2011**, *364*, 86-89.
13. Foresman, J. B.; Frisch, A.; Exploring Chemistry with Electronic Structure Methods. Pittsburgh, PA.: Gaussian Inc., 1993. Print.
14. Fraunhofer Institute for Solar Energy Systems, Photovoltaics Report, ISE https://www.ise.fraunhofer.de/content/dam/ise/de/documents/publications/studies/Photovoltaics-Report.pdf, March 14, 2019.
15. Frisch, M. J. et.al. *Gaussian 03, Revision B.03, Gaussian*, Inc., Pittsburgh PA, 2003
16. Giri, S.; Moore, C. H.; McLeskey, J. T.; Jena, P. Origin of the Red Shift in Photoabsorption Peak in MEH-PPV Polymer. *Journal of Physical Chemistry* **2014,** *118*, 13444-13450.
17. Gong, X. Toward High Perfomance Inverted Polymer Solar Cells. *Polymer* **2012**, *53*, 5437-5448.
18. Heeger, A. Semiconducting and Metallic Polymers: The Fourth Generation of Polymeric Materials (Nobel Lecture), *Angewandte Chemie-International Edition* **2001,** *40*, 2591-2611
19. Hirao, H. Which DFT Functional Performs well in the calculation of Methylcobalamin? Comparison of B3LYP and BP86 Functionals and Evaluation of the impact of empirical dispersion correction. *The Journal of Physical Chemistry A*, **2011**, *115*, 9308-9313.
20. Hochstrasser, R. M.; Kasha, M. Application of the exciton model to mono-molecular lamellar systems. *Photochemistry and Photobiology* **1964**, *3*, 317-331.
21. Huo, L.; Zhang, S.; Guo, X.; Xu, F.; Li, Y.; Hou, J. Replacing Alkoxy Groups with Alklthienyl Groups: A Feasible Approach to Improve the Properties of Photovoltaic Polymers. *Agnew Chem., Int. Ed.* **2011**, *50*, 9697-9702.
22. International Energy Outlook 2013, US Energy Information Administration, Report Number DOE/EIA-0484(2013)

23. Kasha, M. Energy Transfer Mechanisms and the Molecular Exciton Model for Molecular Aggregates. *Radiation Research* **1963**, *20*, 55-71.
24. Kastinen, T.; Niskanen, M.; Risko, C.; Cramaric, O.; Hukka, T. I.; On describing the optoelectronic characteristics of poly(benzodithiophene-co-quinoxaline)- fullerene complexes: the influence of optimally tuned density functionals. *Phys. Chem. Chem. Phys.* **2016**, *18*, 27654-27670.
25. Kityk, A. V.; Charge transfer optical absorption and fluorescence emission of 4-(9-acridyl)julolidine from long-range-corrected time dependent density functional theory in polarizable continuum approach. *Spectrochimica Acta Part A: Molecular and Biomolecular Spectroscopy,* **2014**,*128*, 370-376.
26. Kohler, A., Hoffman, S. T. and Bassler, H. An order-Disprder Transition in Conjugated Polymer MEH-PPV. *Journal of American Chemical Society* **2012,** *134*, 11504-11601.
27. Korzdorfer, T.; Sears, J. S.; Sutton, C.; Bredas, J. Long-range corrected hybrid functionals for π-conjugated systems: Dependence of range-separation parameter on conjugation length. *Journal of Chemical Physics* **2011**, *135*, 204107.
28. Lampert, Z.E.;Reynolds,C. L.; Papanikolas, J. M.; Aboelfohoh, M. O. Controlling Morphology and Chain Aggregation in Semiconducting Conjugated Polymers: The role of solvent on Optical Gain in MEH-PPV. *Journal of Physical Chemistry* **2014**,*116*, 12835-12841.
29. Lima, I. T.; Risko, C.; Aziz, S. G.; da Silva Filho, D. A.; Bredas, J. Interplay of alternative conjugated pathways and steric interactions on the electronic and optical properties of donor-acceptor conjugated polymers. *Journal of Materials Chemistry C*, **2014**, *2*, 8873-8879.
30. Liu, X.; Zhao, S.; Xu, Z.; Zhang, F.; Zhang, T.; Gong, W.; Yan, G.; Kong, C.; Wang, Y.; Xu, X. Performance improvement of MEH-PPV:PCBM solar cells using bathocuproine and bathophenenthroline as the buffer layers. *Chinese Physics B* **2011,** *20,* 10.1088/1674-1056/20/6/068801.
31. McCormick, T. M.; Bridges, C. R.; Carrera, E.I.; DiCarmine, P. M.; Gibson, G. L.; Hollinger, J.; Kozycz, L. M.; Seferos, D. S. Conjugated polymers: evaluating DFT

methods for more accurate orbital energy modeling. *Macromolecules*, **2013**, *46*, 3879-3886.

32. Nagata, S.; Atkinson, G.; Pestov, D.; Tepper, G.; McLeskey, J. Electrospun Polymer-Fiber Solar Cell, *Advances in Material Science and Engineering*, **2013**, Article ID 975947, 6 pages
33. Nenon, S.; Champagne, B.; Spassova, M. I. Assessing long-range corrected functionals with physically-adjusted range-separated parameters for calculating the polarizability and second hyperpolarizability of polydiacetylene and polybutatriene chains. *Phys. Chem. Chem. Phys.* **2014**, *16*, 7083-7088.
34. Nguyen, T. Q.; Doan, V.; Schwartz, B. J. Conjugated polymer aggregates in solution: Control of interchain interactions. *Journal of Chemical Physics* **1999**, *110,* 4068-4078.
35. Paier, J.; Marsman, M.; Kresse, G. Why does the B3LYP hybrid functional fail for metals? *The Journal of Chemical Physics,* **2007,** *127,* 024103.
36. Pandey, L.; Doiron, C.; Sears, J. S.; Bredas, J. Lowest excited states and optical absorption spectra of donor-acceptor copolymers for organic photovoltaics: a new picture emerging from tuned long-range corrected density functionals. *Phys. Chem. Chem. Phys.* **2012**, *14,* 14243-14248.
37. Po, R.; Maggini, M.; Camaioni, N. Polymer Solar Cells: Recent Approaches and Achievements. *Journal of Physical Chemistry C* **2010**, *114*, 695-706.
38. Potai, R.; Traiphol, R. Controlling chain organization and photophysical properties of conjugated polymer nanoparticles prepared by reprecipitation method: The effect of initial solvent, *Journal of Colloid and Interface Science*, **2013**, *403*, 58-66
39. PVEducation.org, Standard Solar Spectra, https://www.pveducation.org/pvcdrom/appendices/standard-solar-spectra, 2019.
40. Quan, S.; Teng, F.; Xu, Z.; Lei, Q.; Hou, Y.; Wang, Y.; Xu, X. Solvent and Concentration Effects on fluorescence emission in MEH-PPV solution. *European Polymer Journal* **2006**, *42*, 228-233.
41. Refaely-Abramson, S.; Baer, R.; Kronik, L. Fundamental and excitation gaps in molecules of relevance for organic photovoltaics from optimally tuned range-separated hybrid functional. *Physical Review B* **2011**, *84,*075144-1-8.

42. Saricifici, N. S.; Smilowitz, L.; Heeger, A. J.; Wudl, F. Photoinduced Electron Transfer from a Conducting Polymer to Buckminsterfullerene. *Science* **1992**, *258*, 1474-1476.
43. Scalmani, G.; Frisch, M. J.; Mennucci, B.; Tomasi, J.; Cammi, R.; Barone, V. Geometries and properties of excited states in the gas phase and in solution: Theory and application of a time-dependent density functional theory polarizable continuum model. *J. Chem. Phys.* **2006,** *124*, 094107: 1-15.
44. Schwartz, B. J. Conjugated Polymers as Molecular Materials: How Chain Conformation and Film Morphology Influence Energy Transfer and Interchain Interactions. *Annual Review of Physical Chemistry* **2003**, *54,* 141-172.
45. Sekar, N.; Katariya, S.; Rhyman, L.; Alswaidan, I. A.; Ramasami, P. Molecular and NLO properties of Red Flourescent Coumarins-DFT Computaions Using Long-Range Separated and Conventional Functionals. *Journal of Fluorescence* **2018**, *10895-018-2333-1.*
46. Small, C.; Tsang, S. W.; Chen, S.; Baek, S. Amb, C.; Subbiah, J.; Reynolds, J.; So, F. Loss Mechanisms in Thick-Film Low-Bandgap Polymer Solar Cells. *Advanced Engineering Materials* **2013**, *3*,909-916.
47. So, W. Y.; Hong, J.; Kim, J. J.; Sherwood, G. A.; Chacon-Madrid, K.; Werner, J. H.; Shreve, A. P.; Peteanu, L. A.; Wildeman, J. Effects of Solvent Properties on the Spectroscopy and Dynamics of Alkoxy-Substituted PPV Oligomer Aggregates. *Journal of Physical Chemistry B* **2012,** *116*, 10504-10513.
48. Solar Energy Perspectives Executive Summary, OECD/IEA, 2011, 19-22
49. Spano, F. C.; Silva, C. H- and J- Aggregate Behavior in Polymeric Semiconductors. *Annual Review of Physical Chemistry* **2014**, *65*, 477-500.
50. Tilley, A.; Danczk, S.; Browne, C.; Young, T.; Tan, T.; Ghiggino, K.; Smith, T.; White, J. Synthesis and Flourescence Characterization of MEH-PPV Oligomers. *Journal of Organic Chemistry* **2011**, *76*, 3372-3380.
51. Tomasi, J.; Mennucci, B.; Cammi, R. Quantum mechanical continuum solvation models. *Chem. Rev.* **2005,** *105,* 2999-3093.

52. Traiphol, R.; Charoenthai, N.; Srikhirin, T.; Kerdcharoen, T.; Osotchan, T.;Maturos, T. Chain organization and photophysics of conjugated polymer in poor solvents: Aggregates, agglomerates and collapsed coils. *Polymer* **2007**, *48*, 813-826.
53. Traiphol, R.; Potai, R.; Charoethai, N.; Srikhin, T.; Kerdcharoen, T.; Osotchan, T. Effects of Chain Conformation and Chain Length on Degree of Aggregation in Assembled Particles of Conjugated Polymer in Solvent-Nonsolvent: A Spectroscopic Study. *Journal of Polymer Science: Part B*, **2010**, *48*, 894-904.
54. US Energy Information Administration; https://www.eia.gov/tools/faqs/, EIA, March 1, 2019.
55. Varian Cary 50 UV-Vis Spectrophotometer specification sheet https://www.agilent.com/cs/library/specifications/Public/si-0821.pdf
56. Weir, B. A.; Marseglia, E. A.; Chang, S. M.; Holmes, A. B. Changes in Structure and Morphology in the conjugated polymer MEH-PPV. *Synthetic Materials* **1999**, *101*, 154-155.
57. Yamagata, H.; Spano, F. C. Interplay between intrachain and interchain interactions in semiconducting polymer assemblies: The HJ-aggregate model. *Journal of Chemical Physics* **2012**, *136,* 184901.
58. Yanai, T.; Tew, D. P.; Handy, N. C. A new hybrid exchange-correlation functional using the Coulomb-attenuated method (CAM-B3LYP). *Chemical Physics Letters* **2004**, *393*, 51-57.
59. Yang, C. Y.; Hide, M.; Diaz-Garcia M. A.; Cao, Y. Microstructure of thin films of photoluminescent semiconducting polymers. *Polymer* **1998**, *39*, 2299-304.
60. Zahid, F.; Saad, P.; Mahmood, M. Solvent Effects on the Electrical and Optical Properties of Nanocomposited MEH-PPV:TiO2 Films for Organic Solar Cells Application. *Advance Materials Research* **2012,** *364*, 86-89.
61. Zang, F. L.; Johansson, M.; Anderson, M. R.; Hummelen, J. C.; Inganas, O. Polymer Solar Cells Based on MEH-PPV and PCBM. *Synthetic Materials* **2003**, *137*, 1401-1402.
62. Zayana, N. Y.; Rusop, M. Effect of Different Solvents on the Optical Properties and Surface Morphology of MEH-PPV Thin Films. *Advanced Materials Research* **2013**, *667*, 402-406.

63. Zheng, M.; Fenglian, B.; Zhu,D. Photophysical process of MEH-PPV solution. *Journal of Photochemistry and Photobiology A: Chemistry* **1998**, *116*, 143-145.
64. Zhong, W.; Li, F.; Chen, L.; Chen, Y.; Wei, Y. A novel approach to electropinning of pristine and aligned MEH-PPV using binary solvents, *Journal of Materials Chemistry*, **2012**, *22*, 5523-5530.
65. Zhu, Z., Zhang, L., Smith, S., Fong, H., Sun, Y.; Gosztola, D. Fluorescence studies of electrospun MEH-PPV/PEO nanofibers. *Synthetic Metals* **2009**, *159*, 1454-1459.